# Towards a hydrogeomorphological understanding of proglacial catchments : an assessment of groundwater storage and release in the Otemma catchment

Tom Müller[1,2], Stuart N. Lane[1], and Bettina Schaefli[1,2,3]

[1]Institute of Earth Surface Dynamics, Lausanne, University of Lausanne, Switzerland
[2]Institute of Geography (GIUB), University of Bern, 3012 Bern, Switzerland
[3]Oeschger Centre for Climate Change Research (OCCR), University of Bern, 3012 Bern, Switzerland

**Correspondence:** Tom Müller (tom.muller.1@unil.ch)

**Abstract.** Proglacial margins form when glaciers retreat and create zones with distinctive ecological, geomorphological and hydrological properties in Alpine environments. There is extensive literature on the geomorphology and sediment transport in such areas as well as on glacial hydrology, but there is much less research into the specific hydrological behavior of the landforms that develop after glacier retreat in and close to proglacial margins. Recent reviews have highlighted the presence of groundwater stores even in such rapidly draining environments. Here, we describe the hydrological functioning of different superficial landforms within and around the proglacial margin of the Otemma glacier, a temperate Alpine glacier; we characterize the timing and amount of the transmission of different water sources (rain, snowmelt, ice melt) to the landforms and between them; and we compare the relationship between these processes and the catchment-scale discharge. The latter is based upon a recession-analysis based framework. In quantifying the relative groundwater storage volumes of different superficial landforms, we show that steep zones only store water on the timescale of days, while flatter areas maintain baseflow in the order of several weeks. These landforms themselves fail to explain the catchment-scale recession patterns; our results point towards the presence of an unidentified storage compartment of the order of 40 mm, which releases water during the cold months. We propose to attribute this missing storage to deeper bedrock flowpaths. Finally, the key insights gained here into the interplay of different landforms as well as the proposed analysis framework are readily transferable to other similar proglacial margins and should contribute to a better understanding of the future hydrogeological behavior of such catchments.

**Keywords.** glacier forefield, hydrology, groundwater storage, recession analysis, review, Alps, Switzerland

## 1 Introduction

Glaciated catchments are highly dynamic systems characterized by complex physical, chemical and biological interactions at multiple scales ranging from local processes in the glacier ice to regional effects transmitted from the glacier forefield to downstream regions (Miller and Lane, 2018; Carrivick and Heckmann, 2017). In such environments, where nutrients and energy are limited and climate variations are large, glaciers provide water (Huss et al., 2017), sediments (Hallet et al., 1996) and organic carbon (Brighenti et al., 2019) to downstream areas, which sustain a high regional biodiversity (Milner et al., 2009). At the regional scale, glaciers provide a number of ecological services essential for human society, such as water supply for drinking water purposes and irrigation, hydropower or cultural services (Beniston et al., 2018; Haeberli and Weingartner, 2020). Water resource availability is undergoing strong seasonal modifications due to climate warming with rapid glacier retreat worldwide (Milner et al., 2017), e.g. an estimated volume loss of 84±15% by 2100 in the European Alps (Huss et al., 2017). Peak annual runoff from glacier melt will be reached between 2010 and 2060 across the world (Huss and Hock, 2018) and the subsequent reduction of ice available to melt, together with more liquid precipitation and earlier snowmelt (Lane and Nienow, 2019; Klein et al., 2016) will cause a change of streamflow regimes, with a shift in the flow magnitude and of the timing of high flows to earlier months (Berghuijs et al., 2014; Beniston et al., 2018; Gabbi et al., 2012; Lane and Nienow, 2019).

Whilst numerous discussions of the implications of cryosphere changes have been published (e.g., Beniston et al., 2018; Huss et al., 2017; Immerzeel et al., 2020), the role of groundwater is typically neglected in many glacio-hydrological studies in Alpine environments (Vuille et al., 2018). This is surprising given the rapidly growing body of literature on groundwater–snowmelt interactions. e.g. for environments with regular droughts (Fayad et al., 2017; Jefferson et al., 2008; Van Tiel et al., 2021), as well as regional studies highlighting large groundwater contributions to streamflows in the Andes (Vuille et al., 2018) and in the Himalayas (Andermann et al., 2012; Yao et al., 2021). Recent studies started to tackle this issue by estimating groundwater contribution at the catchment-scale or by analyzing the hydrological processes of specific landscape units. At the catchment-scale, water stable isotopes as well as other geochemical tracers were used to identify groundwater contributions of 20% to 50% for sub-catchments having a 25% to 4% glaciated cover (Penna et al., 2017; Engel et al., 2016, 2019). While those studies provide interesting insights into the role of groundwater to sustain baseflow, the allocation of storage to specific hydrological units remain unclear. This is problematic as such systems are subject to rapid geomorphological changes, with large areas of previously ice-covered till and bedrock becoming exposed in proglacial margins (Heckmann and Morche, 2019), leading to the emergence of new landforms prone to groundwater storage (Hayashi, 2020). Thus, studies focusing on the integrated catchment-scale response provide little information on the internal mechanisms which maintain baseflow, and they therefore cannot predict the future changes of groundwater storage and its contribution to streamflow.

Other studies have approached this issue by characterizing the structure and hydrological response of specific geomorphological units in terms of water partitioning, storage and release (Wagener et al., 2007). Those unconsolidated superficial landforms are formed by different glacial and slope processes, have different internal structures and sedimentology and create a complex mosaic of landforms in glaciated catchments, which we summarize in Fig. 1.

A recent comprehensive study of the hydrogeological processes in such geomorphological landforms was provided in the work of Hayashi (2020). Here, we only retain some key information. Morainic material can be deposited both on slopes or in flatter areas. They are composed of a non-sorted mix of fine to coarse materials, which may contain more consolidated till (Ballantyne, 2002). Where they are in contact with a stream network, complex interactions occur and relatively deep aquifers (10 m depth) can be formed, which may sustain baseflow during dry periods (Magnusson et al., 2014; Kobierska et al., 2015b). Heavily debris-covered relict glaciers lead to the formation of rock glaciers. They were shown to consist mainly of a coarse layer with high hydraulic conductivity but contain a 1 to 2 m basal layer of finer water-saturated sediments, which can store significant water amounts (Harrington et al., 2018; Winkler et al., 2016; Wagner et al., 2021). In flat valley bottoms, fluvial

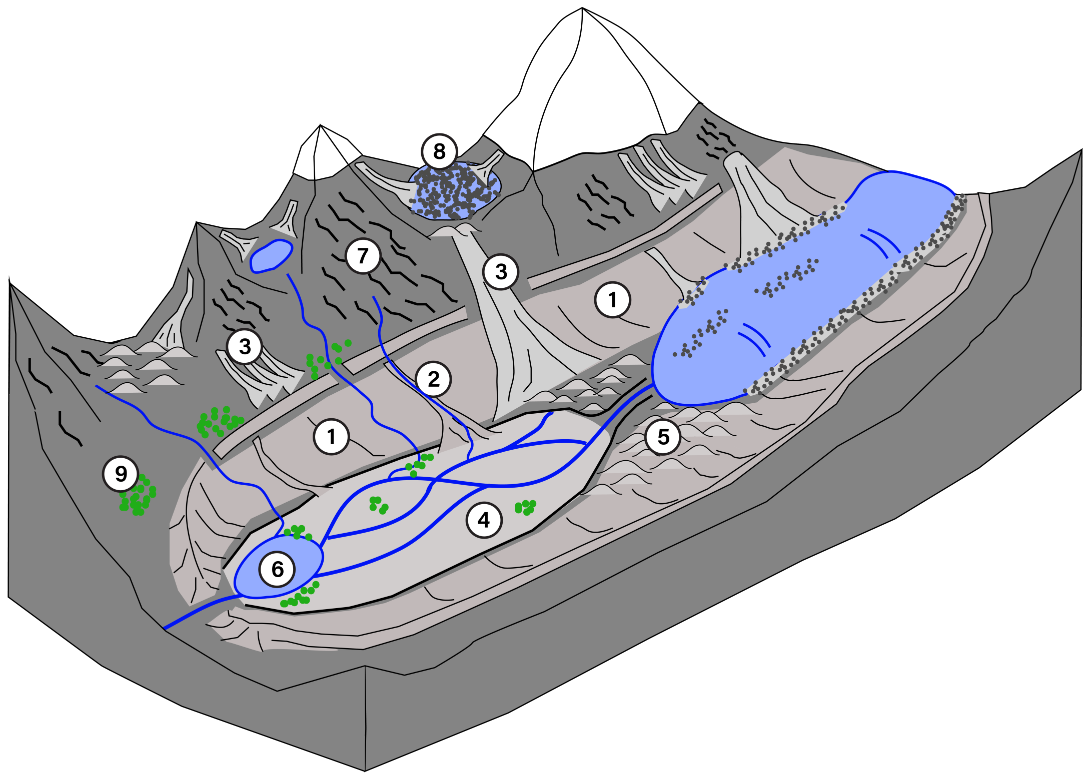


**Figure 1.** General overview of geomorphological landforms typical of proglacial zones. 1) Lateral moraine (grey); 2) Debris cone; 3) Talus slope (light grey); 4) Fluvial outwash plain; 5) Glacial deposit (till) ; 6) Proglacial lake ; 7) Apparent bedrock (dark grey); 8) Debris-covered rock glacier; 9) vegetation patches. Snow on the mountain tops is in white and the glacier is in blue on the right. (figure inspired from Temme (2019))

deposition of sandy-gravelly material will lead to the creation of so-called glaciofluvial outwash plains (Maizels, 2002). They collect water from multiple sources and maintain groundwater-fed river channels in autumn, promoting habitat heterogeneity and high local biodiversity (Ward et al., 1999; Malard et al., 1999; Crossman et al., 2011; Hauer et al., 2016). Older outwash plains were shown to have strong interactions with glacier-fed streams (Ó Dochartaigh et al., 2019; Mackay et al., 2020) and to provide upward groundwater exfiltration contributing between 35 and 50% to river baseflow (Käser and Hunkeler, 2016; Schilling et al., 2021). On hillslopes, debris not linked to glaciogenic origin come from rock slope failures, leading to the formation of talus slopes. These talus slopes are composed of coarser debris than morainic material, showing thereby little water retention capacity and fast water transfer to downstream units (Muir et al., 2011).

Those studies provide key information on the groundwater dynamics of selected units; they are, however, rarely integrated into a perceptual model that brings together knowledge of all units, that compares their relative storage volumes and their contribution to streamflow and that thereby explains the overall catchment-scale hydrological response. To our knowledge, only a limited number of studies propose an integrated description of the hydrogeological behavior of proglacial margins: in the Canadian Rockies a series of papers studied the hydrogeology of different proglacial structures and were summarized in the work of Hayashi (2020); in the Cordillera Blanca in Peru a suite of studies (Baraer et al., 2015; Gordon et al., 2015; Somers et al., 2016; Glas et al., 2018) focused on the role of groundwater for stream flow in different proglacial valleys; and in the Swiss Alps, there is a review of the hydrological behavior of proglacial landforms by Parriaux and Nicoud (1990).

From our perspective, but as also highlighted by others (Heckmann et al., 2016; Vincent et al., 2019), there is still a need for integrative studies that (i) document the hydrological functioning of proglacial landforms with appropriate metrics; (ii) propose a framework to characterize the timing, amount and location of the transmission of different water sources (rain, snow, ice) to these landforms and between each of them; (iii) compare if the documented response of individual landforms can explain the observed catchment-scale behavior in terms of streamflow amounts, timing and geochemistry ; (iv) propose a unifying theory for the geomorphological, ecological and hydrological evolution of such rapidly evolving catchments.

Within this paper, we propose a framework to address the first three of above-mentioned points. First, we present field observations from the Otemma glaciated catchment, our case study in the Swiss Alps (Sect. 2.1) and discuss the different hydrological behaviors observed around the outwash plain, based on electrical conductivity data, direction of groundwater flowpaths and an estimation of hydraulic conductivity (Sect. 3.1). We then propose a methodology to characterize the hydrological behavior of the different superficial landform storages by assessing their storage-discharge relationship based on recession analysis and a literature review of the time scales of their hydrological response (Sect. 3.3). Applied to our case study, we quantify the seasonal storage and discharge capacity for each landform with a simple model (Sect. 3.5). Finally, we perform a mutli-year recession analysis at the catchment outlet to analyze the catchment-scale hydrological response (Sect. 3.2) and compare the estimated catchment-scale storage with the storage of each landform obtained from the previous analysis.

## 2 Study site and experimental methods

### 2.1 Site description

With an ice-covered area of about 14 km$^2$, the Otemma glacier ($45°56'3''$N,$7°24'42''$E) in the Western Swiss Alps is amongst the 15 largest glaciers of Switzerland (Fischer et al., 2014). The glacier is characterized by a relatively flat tongue, which has retreated by about 2.3 km since the Little Ice Age (LIA) and 50 m year$^{-1}$ since 2015 (GLAMOS (1881-2020)). A recent study suggested an almost complete glacier retreat by 2060 (Gabbi et al., 2012).

A Tyrolean-type water intake (GTZ, 1989) has been constructed for hydropower production about 2.5 km downstream of the current glacier terminus and is used in the present study as the outlet of what we call the Otemma basin (Fig. 2). It has an area of 30.4 km$^2$, a mean elevation of 3005 m a.s.l. (2350 m to 3780 m) and a glacier coverage of 45% in 2019 (adapted from GLAMOS (1881-2020)).

The geology of the underlying bedrock is composed of gneiss and orthogneiss from the Late Paleozoic Era with some granodiorite inclusions (GeoCover - Federal Office of Topography). The main geomorphological forms comprise bedrock, with some vegetation cover above the LIA limit (46%), steep slopes (30% post-LIA lateral moraines and 10% talus slopes),

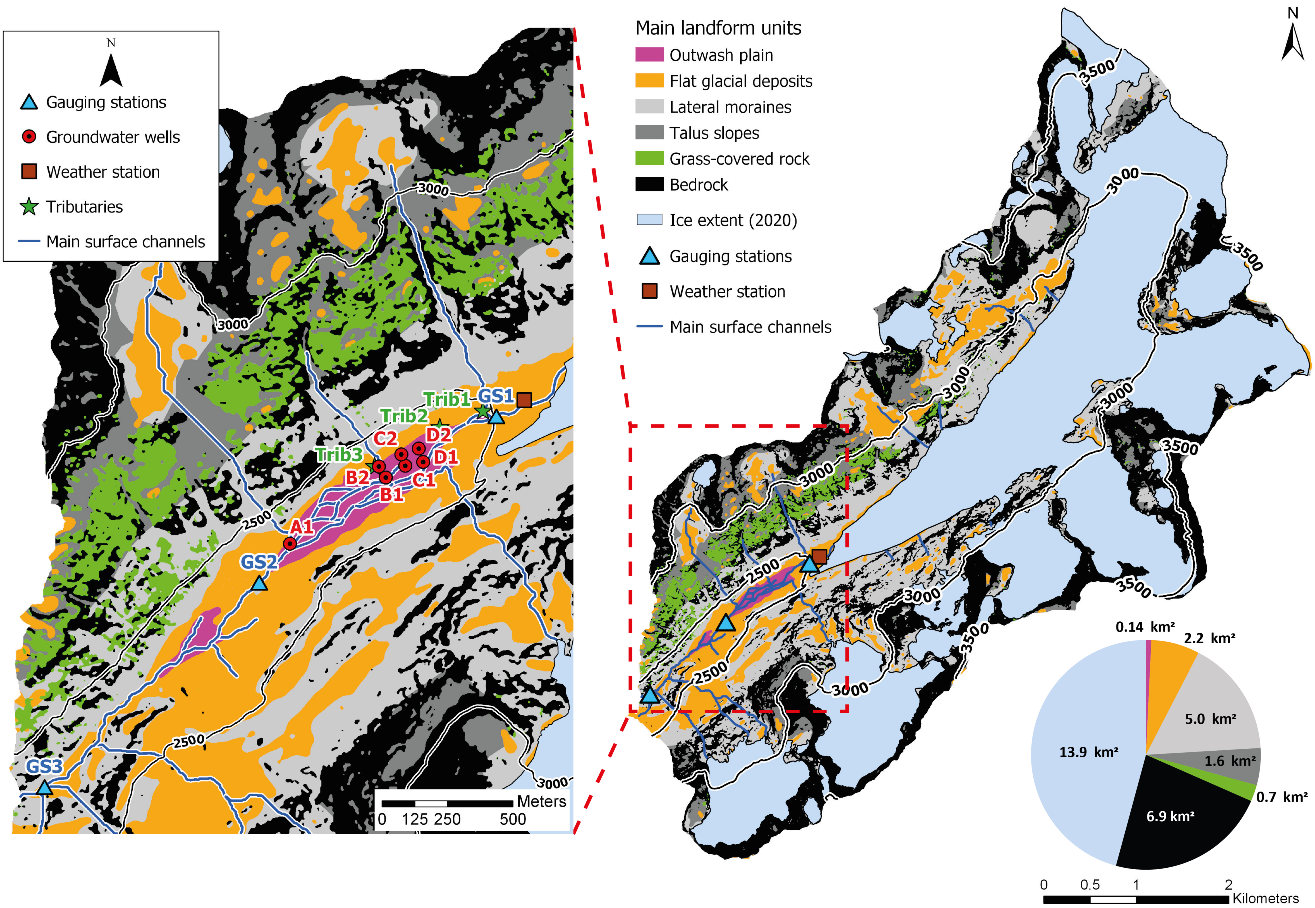


**Figure 2.** Overview of the Otemma catchment classified based on its main geomorphological landforms (see 3.4) and the location of the gauging stations (GS) and weather station. The pie chart shows the surface area of each unit. The zoom-in window on the left shows the field measurements stations installed between 2019 and 2021. The outwash plain is located between gauging stations 1 and 2 (GS1 and GS2).

gently sloping debris fans and morainic deposits (13%) and a flat glaciofluvial outwash plain (0.9%) (Fig. 2). One main subglacial channel at the glacier snout provides water to a large, highly turbid and turbulent stream, which quickly reaches a flat outwash plain composed of sandy-gravelly sediments; this leads to a braided river network, which eventually converges in a more confined channel about 1 km downstream and extends to the hydropower intake. A few tributaries from small hanging glaciers or valleys also contribute to river discharge during the snow-free season.

## 2.2 Hydrometeorological data

Since July 2019, we installed an automatic weather station (Fig. 2) at the glacier snout at an elevation of 2450 m a.s.l., continuously recording air temperature, humidity, atmospheric pressure (Decagon VP-4) and liquid precipitation (Davis tipping rain gauge). Since July 2020, total incoming shortwave radiation was also recorded by the device (Apogee SP-110). Winter solid precipitation data were provided by SwissMetNet, the Swiss automatic monitoring network, using information from the Otemma station (2.7 km from glacier snout) or the Arolla station (10 km from glacier snout). Data with a detailed description is available on Zenodo (Müller, 2022a).

### 2.3 Hydrological data

Since 2006, hourly river stage was recorded at the water intake corresponding to our catchment outlet ($GS3$, see zoom-in in Fig. 2) by the local hydropower company (Force Motrice de Mauvoisin, FMM); corresponding discharge was estimated using a theoretical stage-discharge relationship provided by FMM. We post-processed the data by in-filling data gaps related to regular sediment flushing events (of a duration <1h) with linear interpolation. Winter discharge was also recorded, although a data gap usually occurred from October to December.

Since August 2019, we installed three river gauging stations, one in the vicinity of the glacier snout (GS1), one at the end of the outwash plain (GS2) and one at the catchment outlet (GS3) (see zoom-in in Fig. 2). River stage, water electrical conductivity (EC) and water temperature were recorded continuously at 10 minutes intervals using an automatic logger (Keller DCX-22AA-CTD). Periodic EC and discharge measurements were also made in many tributaries and water sources, with a main focus on three representative tributaries along the outwash plain. Finally, we installed 7 groundwater wells consisting of fully screened plastic tubes at an averaged depth of 1.5 to 2 m in the outwash plain, which covered four transects (A to D) perpendicular to the river in the direction of the base of the hillslope. Watertable elevation was recorded in each well at a 10 minutes interval using SparkFun MS5803-14BA pressure sensors. Sensor bias was verified and corrected by bi-monthly manual groundwater stage measurements. More detailed description of the data is available on Zenodo (Müller and Miesen, 2022).

### 2.4 Electrical resistivity tomography

Electrical resistivity tomography (ERT) was used to map the sediment structure in the outwash plain. We performed a total of 21 lines from 2019 to 2021 using a Syscal Pro Switch 48 from Iris Instruments. The electrode array consisted of 48 electrodes with a spacing between 1.5 to 4 m and Dipole-Dipole (DD) and Wenner-Schlumberger (WS) schemes were systematically used for better data interpretation. We processed the data using the Open-Source pyGIMLi python library (Rücker et al., 2017). All data inversions were calculated with different regularization parameters to assess over and underfitting. The depth of the outwash plain sediments was measured by performing multiple transects and by identifying the transition from water-saturated sediments having a resistivity value between 500 to 2000 $\Omega m$ and the bedrock layer with a resistivity of 4000 to 7000 $\Omega m$, similarly to other studies (e.g. Langston et al., 2011; Harrington et al., 2018). More detailed description of the data is available on Zenodo (Müller, 2022c).

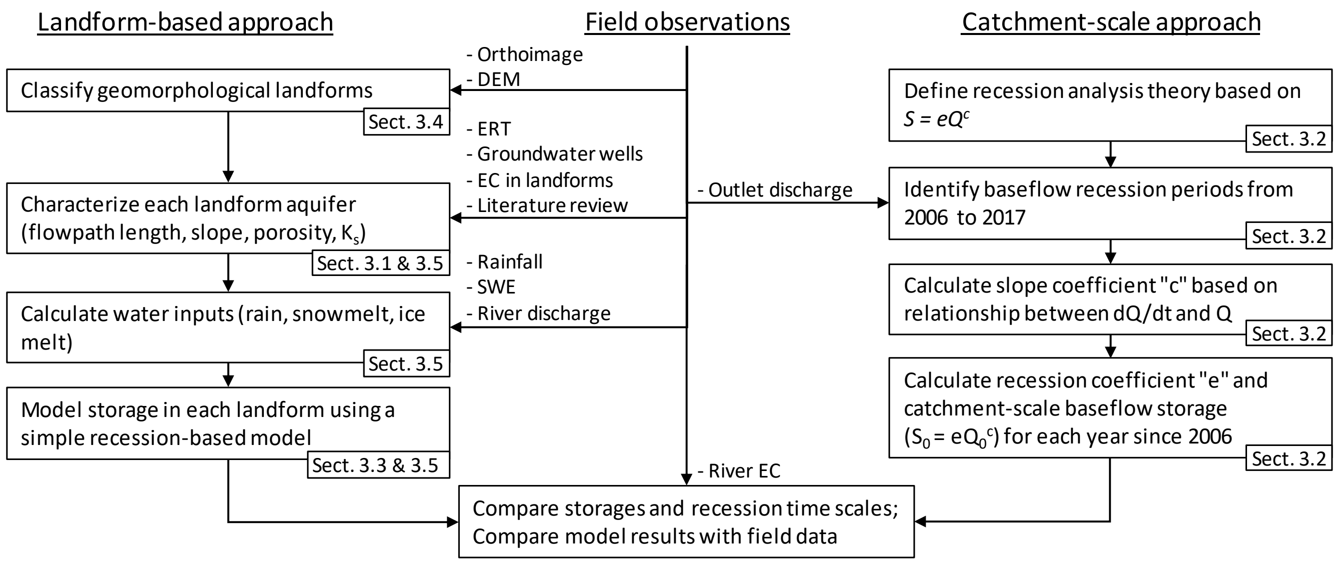


**Figure 3.** Sketch of the adopted workflow, separated between field observations, landform-based and catchment-based methods. The corresponding sections in the methodology are also highlighted. All abbreviations are detailed in the text.

## 3 Methods

We propose in this study to use two frameworks based on recession theory to analyze both the catchment-scale hydrological response and the response of individual landforms. These two approaches are applied on our case study in the Swiss Alps using various field data and we ultimately compare the results obtained from both methods together and against field observations. The workflow of the overall methodology is summarized in Fig. 3.

### 3.1 Estimation of hydraulic conductivity in the outwash plain

While some literature exists to characterize most geomorphological landforms in glaciated catchments, data on post LIA outwash plains in alpine environments are scarce. We therefore used two different methods to estimate the saturated hydraulic conductivity ($K_s$) of the outwash plain.

The first method applies the pressure wave diffusion method documented in the work of Magnusson et al. (2014). Given a certain hydraulic diffusivity ($D$), this method relates the aquifer head variations ($h$) at a distance $x$ from the stream, to the diel stream stage cycles ($h_{x=0}$) generated by ice melt. It furthermore makes use of a simplified 1D Boussinesq equation, where advective fluxes are neglected (Eq. 1). This procedure is only valid for relatively flat aquifers with a thick unconfined saturated layer and where evapotranspiration losses can be neglected (Kirchner et al., 2020), which makes this approach well-suited for high elevation outwash plains. By comparing the phase shift (time lag) and the amplitude dampening between the river stage and the groundwater signals, the aquifer hydraulic diffusivity ($D$) can be estimated and related to $K_s$ using the aquifer thickness ($B$) and assuming that the specific yield ($S_y$) is similar to the aquifer porosity (Eq. 2).

$$\frac{\delta h}{\delta t} = D\frac{\delta^2 h}{\delta x^2} \tag{1}$$

$$D = \frac{K_s B}{S_y} \tag{2}$$

For this analysis, we used the two upstream and downstream well transects ($B$ and $D$, see Fig. 2) for two periods: during high flow in mid-August 2019 and during a lower flow period in mid-September 2019. An additional groundwater well "B3" on the transect $B$ was also used for this analysis. The 1D partial differential equation was solved using a central-differencing scheme in space and a Crank-Nicolson method in time, imposing the measured river stage variations as a boundary condition. Prior to solving the equation, both river stage and groundwater heads were detrended by substracting the linear trend of each dataset as suggested by Magnusson et al. (2014). We then calibrated the model parameter $D$ using a Monte-Carlo approach where we minimized the root mean square error and maximized the Spearman rank correlation between observed and modelled groundwater heads. Hydraulic conductivity was finally calculated based on the aquifer thickness measured by ERT and porosity was estimated by measuring saturated water content (Decagon 5TM) at five locations in the upper sediment layer.

A second independent estimation of the hydraulic conductivity was obtained with salt tracing, using ERT time-lapse with a measurement cycle of about 30 minutes. We injected 3 kg of salt dissolved in 15 L of water in a 1 m deep pit in the center of the outwash plain, and recorded the timing of the passage of the salt plume at a downstream transect (distance 9.38 m) using ERT, similarly to the work of Kobierska et al. (2015a). We only installed one ERT line perpendicular to the groundwater flow consisting of 48 electrodes with a 1 m spacing. Hydraulic conductivity can be calculated by solving Darcy's Law for the mean pore velocity as follows:

$$v_p = \frac{K_s}{\theta_s}\frac{dh}{dx}, \tag{3}$$

where $\frac{dh}{dx}$ is the aquifer gradient, $\theta_s$ is the aquifer porosity and $v_p$ is the mean pore velocity corresponding to the travel distance divided by the travel time of the center of gravity of the salt plume.

### 3.2 Catchment-scale recession analysis

We analyze the storage-discharge relationship at the catchment-scale with a classical recession analysis during periods when both water inputs (snow, rain) as well as outputs (evapotranspiration) can be neglected, i.e. during periods when discharge is only related to aquifer storage (Kirchner, 2009; Clark et al., 2009). Following Kirchner (2009), we describe the recession behavior of the aquifer storage with a non-linear storage ($S$)-discharge ($Q$) function:

$$S = eQ^c \tag{4}$$

whose derivative, using $\frac{dS}{dt} = -Q$ is given by :

$$-\frac{dQ}{dt} = \frac{1}{ce}Q^{(2-c)} \tag{5}$$

This is usually summarized as $-\frac{dQ}{dt} = aQ^b$, where $a = 1/ce$ is the recession coefficient and $b = 2 - c$ is the slope coefficient (Santos et al., 2018). The release behavior of the catchment-scale storage can be characterized by identifying zones where the slope of the relationship between the rate of change ($-\frac{dQ}{dt}$) and discharge ($Q$) is constant in the logarithmic scale, which allows calculation of the slope coefficient $b$.

We perform the recession analysis for the 12 years period of discharge data provided by FMM at the catchment outlet (GS3). The recession periods are automatically selected by identifying periods where flow is constantly decreasing for at least 10 days and is extended until the first increase in flow. The discharge recession data were smoothed (moving average with a span of 50% of a given recession period) to remove small step-like decreases or small drops due to sensor failures, so that only the averaged trends are analyzed. Finally, we plot the relationship between ($-\frac{dQ}{dt}$) and discharge ($Q$) and we average the recession points from all years in bins with an equal number of points (we selected 100), as suggested in the work of Kirchner (2009) on which we apply a linear regression (Nonlinear Least Squares method, Matlab R2019a). This procedure allows estimation of the slope coefficient $b$. Once $b$ is identified, we fit a power law function on the raw discharge data (without any smoothing) for each winter recession, using the analytical solution of Eq. (5) in order to estimate the recession coefficient $e$. Finally, this allows us to relate the maximum baseflow discharge $Q_0$ to the catchment-scale baseflow storage $S_0$ using Eq. (4).

### 3.3 Assessing the hydrological response based on aquifer characteristics and recession analysis

Similarly to the catchment-scale recession analysis, the same relationship between storage and discharge can be applied to specific landforms, which allows to estimate the rate of water storage and release in different parts of a glaciated catchment. For instance, the form of the water table in an aquifer can be linked to the shape and physical properties of the landform (Troch et al., 2013). Using some simplifications, the Boussinesq equation (Boussinesq, 1904) proposes a physically-based equation for the temporal variation of the aquifer table along a one directional aquifer and thus allows estimation of discharge based on the groundwater gradient and physical properties of the aquifer (Harman and Sivapalan, 2009a).

For flat aquifers with homogeneous conductivity, a slope $b$ of 1.5 ($c$=0.5) is common for the late recession (Rupp and Selker, 2006). Such a value can be obtained using an analytical solution of the Boussinesq equation and leading to the discharge solution (Wittenberg and Sivapalan, 1999; Rupp and Selker, 2005) shown in Eqs. (6) & (7):

$$S = eQ^{0.5} \tag{6}$$

$$Q_t = Q_0(1+\alpha t)^{-2} \tag{7}$$

$$\alpha = \frac{Q_0^{0.5}}{e} \approx \frac{K_s h_m}{\phi L^2}. \tag{8}$$

A physical description of $\alpha$ can be proposed (Eq. 8) based on the aquifer conductivity ($K_s$) and porosity ($\phi$), the aquifer length ($L$) and the aquifer thickness at distance $L$ ($h_m$) (Dewandel et al., 2003; Rupp and Selker, 2005; Stewart, 2015).

In the case of a significantly slopping aquifer (>10°), a value $b$=1 is usually proposed for the late drainage (Rupp and Selker, 2006; Muir et al., 2011). In this case, if the aquifer thickness is small enough, the aquifer flux is mostly advective and conducted by the bedrock slope (Harman and Sivapalan, 2009b) so that discharge recession becomes linear (Eqs. 9 & 10). Due to the non-linearity of the Boussinesq equation, the parameter $\alpha$ can only be approximated using numerical linearization approaches (Hogarth et al., 2014; Verhoest and Troch, 2000). In this study we use one of the simplest proposed descriptions for $\alpha$ (Eq. 11), similar to the previous one, where only $h_m/L$ (the aquifer slope) is replaced by $sin(\theta)$ and $\theta$ is the bedrock slope (Harman and Sivapalan, 2009a; Berne et al., 2005; Rupp and Selker, 2006).

$$S = eQ \tag{9}$$

$$Q_t = Q_0 \mathrm{e}^{-\alpha t} \tag{10}$$

$$\alpha = \frac{1}{e} \approx \frac{K_s sin(\theta)}{\phi L} \tag{11}$$

In both equations (Eq. 7 & 10), the rate of aquifer decline can be related to a recession constant ($1/\alpha$), corresponding to the characteristic response time of the aquifer. Based on this approach, we review the range of estimated hydraulic conductivity values reported in recent studies for typical landforms in glaciated catchments. Combined with realistic aquifer properties (slope, porosity, aquifer length) for each type of landform, we can apply the proposed relationships for flat (Eq. 8) or sloping aquifers (Eq. 11) and finally assess the recession time scales ($1/\alpha$) at which different storage compartments provide water for baseflow.

### 3.4 Superficial landform classification

Following the procedure described in the previous section, we propose to compare the contribution from each of the main superficial landform storage compartment for the specific case of the Otemma catchment. Landform classification was performed by combining a visible band orthoimage from 2020 with a 10 cm resolution and a 2 m resolution digital elevation model (DEM) provided by Swisstopo. We calculated the slope from the DEM and classified it in categories as suggested in the work of Carrivick et al. (2018) : <8° for outwash plains; 8-22° for mildly sloping glacial deposits and debris cones; 22-42° for lateral moraines below the LIA limit and talus slopes above the LIA limit; >42° for bedrock. We then downscaled the orthimage to 2 m and combined the RGB bands with an additional band corresponding to the slope classes. We manually identified small zones corresponding to the main landform features and performed a supervised classification using a random trees classifier (ArcGIS Pro v2.3). We finally calculated the median class for a moving window of 10 by 10 cells (20x20 m) to smooth out noise in the results. A specific class for grass was used, since many grass patches were identified above the LIA line on shallow soils on top of bedrock. Lateral moraines below the LIA line was distinguished from coarser debris talus slopes with similar slopes in zones where glaciers were absent during the LIA. The glacier extents from 1850 (LIA limit) and 2016 are provided by the Swiss Glacier Inventory 2016 (Linsbauer et al., 2021). The results are presented in Fig. 2.

### 3.5 Landform-based model of the hydrological response of single geomorphological units

We propose here a simple methodology to estimate the seasonal storage and discharge contribution of each individual superficial landform storage compartment in the Otemma catchment based on the recession theory (Sect. 3.3). In order to estimate the maximum water storage, we use the total area ($A_i$) of each classified landform (Sect. 3.4) and an estimation of their sediment thickness, similarly to other studies (Hood and Hayashi, 2015; Rogger et al., 2017). Sediments are however never fully water-saturated, so that it remains difficult to estimate the maximum aquifer thickness for each landform. To overcome this limitation, we define a simple hydrological model where we simulate a realistic daily water input ($Q_{in}$) in the form of rain ($P_{rain}$) and snowmelt ($P_{snow}$) and estimate storage ($S$) and outflow discharge ($Q_{out}$) based on the non-linear storage-discharge relationship (Eq. 4). We define $c$ based on the landform slope and estimate $e$ following Eq. (8) or (11) using realistic hydrological characteristics of each landform: hydraulic conductivity is based on our measurements (Sect. 3.1) or from literature review, while the aquifer slope and length are estimated for each landform based on our landform classification by manually measuring the averaged landform length (Fig. 2).

Following this approach, we define Eqs. (12) to (14) in order to simulate the seasonal storage and discharge over a whole year.

$$\frac{\delta S_t}{\delta t} = Q_{in,t} - Q_{out,t} \tag{12}$$

$$Q_{in,t} = ((P_{snow,t} + P_{rain,t})A_i + Q_{glacier,t})/A_{catchment} \tag{13}$$

$$Q_{out,t} = \left(\frac{S_t}{e}\right)^{1/c} \tag{14}$$

where $\frac{\delta S}{\delta t}$ is the change of storage in mm day$^{-1}$, $Q_{in,t}$ is the daily water input at time $t$ and $Q_{out,t}$ is the generated daily output discharge based on the non linear storage-discharge equation. $P_{snow}$ and $P_{rain}$ are the daily snowmelt and daily liquid precipitation in mm day$^{-1}$, $A_i$ is the area of each landform, $Q_{glacier}$ is the daily river discharge from the glacier in liters day$^{-1}$ and $A_{catchment}$ is the total catchment area in m$^2$. Finally $e$ is the recession parameter estimated based on $\alpha$ (Eq. 8 or 11) and $c$ the slope coefficient (1 for slopping aquifers >10° and 0.5 for flatter aquifers). In these equations, the landform storage ($S_t$) is scaled by dividing the volume by the entire catchment area and allowing to compare the storage of different landforms.

The snowmelt input is modelled with a snow accumulation routine (rain transitions to snow from an air temperature between 1 and 2°C) and a degree day model for daily snowmelt estimation following Gabbi et al. (2014), with a degree-day melt factor of 6.0 mm °C$^{-1}$ day$^{-1}$ when air temperature is higher than 1°C. The catchment was separated in 50 m elevation bands with a calibrated temperature lapse rate of 0.5°C 100 m$^{-1}$ and precipitation lapse rate of +10% 100 m$^{-1}$. Winter precipitation from SwissMetNet were adapted using a correction factor for each year. The melt parameters, precipitation correction factor and lapse rates were estimated by minimizing the error between modelled and observed SWE based on 92 snow depth measurements and two snow pits for density measurements made near the maximum snow accumulation on 28 Mai 2021. It was further calibrated by matching the snowline limit during the snowmelt season as suggested in Barandun et al. (2018), based on daily 3 m resolution Planet images (Planet, 2017). Snowmelt and rain inputs are considered to recharge entirely the whole aquifer (no surface flow) and there is no routing or water exchange between the different landforms, so that our estimates represent the maximum potential storage linked to a realistic maximum recharge.

In the case of the outwash plain, an additional glacier melt input ($Q_{glacier}$) is provided, since this is the only landform directly recharged by the river network in Otemma. Only a small fraction of the total river discharge was allowed to recharge the outwash plain aquifer. An infiltration rate of 100 liters s$^{-1}$ (2% of mean summer discharge) from May to October was used and was estimated from dilution gauging along the stream and preliminary modelling results. This amount was also found to realistically approximate the rate of recharge observed using the groundwater wells. Finally, the maximum storage (sediment thickness) of the reservoirs cannot be exceeded in any landforms.

Based on the three sources of water (rain water, snowmelt, glacial stream), a small routine was also added to calculate the source water partitioning in each landform. At each time step, the reservoir is assumed to be fully mixed and a water amount for each water source is removed, proportional to the estimated partitioning at the previous timestep and so that the total water removed equates the calculated discharge ($Q_{out,t}$). The amount of water recharge from each source is then added and a new partitioning is calculated. This allowed to keep track of the seasonal contribution of different water sources in each landform.

## 4 Results

### 4.1 Water electrical conductivity

#### 4.1.1 Stream observations

Streamflow EC in the Otemma catchment shows strong seasonal and diel cycles driven by snow and glacier melt (Fig. 4). During summer, when discharge is highest, streamflow EC remains very low, with small diel variations of the order of 10 to 20 $\mu\mathrm{S/cm}$ (Fig 4b). During this period, EC is strongly negatively correlated with river discharge, with maximum streamflow EC in the morning. There is an EC increase between the glacier snout (GS1) and the end of the outwash plain (GS2), but hardly any change further downstream (i.e. between GS2 and GS3). After November, EC increases gradually during the whole winter (Fig 4a), until the first onset of snowmelt in early spring. Similar to the summer, there is a difference in EC between GS1 and GS2, which becomes larger as EC at GS1 increases less rapidly in March 2021. A small EC difference between GS2 and GS3 only occurs during the very low flow conditions from mid-November to March.

#### 4.1.2 Hillslope and groundwater observations

We monitored the EC of selected landforms as well as of different water sources. The averaged snowmelt EC was $5.1\pm2.46\,\mu\mathrm{S/cm}$ based on 28 snowpack samples collected during the snowmelt season in the outwash plain and on the glacier surface up to 2850 m a.s.l. Surface ice-melt samples show EC values of $5.7\pm4.3\,\mu\mathrm{S/cm}$ based on 29 samples. The average rain EC value is $31.6\pm11.3\,\mu\mathrm{S/cm}$ based on 11 samples. The reason for a slightly higher EC in rain than snowmelt is not known but has also been reported in other studies (Zuecco et al., 2019).

Tributaries on the side of the outwash plain show only limited change in EC during summer (Fig. 5), but present different trends. Tributary 1 is located below a hanging valley, likely containing buried ice or permafrost and snow at high elevation, leading to a perennial superficial flow. The relatively low EC of this tributary seems to indicate a marginal groundwater contribution, with probably only a short contact time between the morainic material and melt water in the higher part of the catchment. Tributary 2 exfiltrates from sediments at the base of the lateral moraine and its EC is only slightly higher than the bedrock exfiltration, suggesting that this tributary is mainly fed by water stored in the bedrock which infiltrates in the coarse

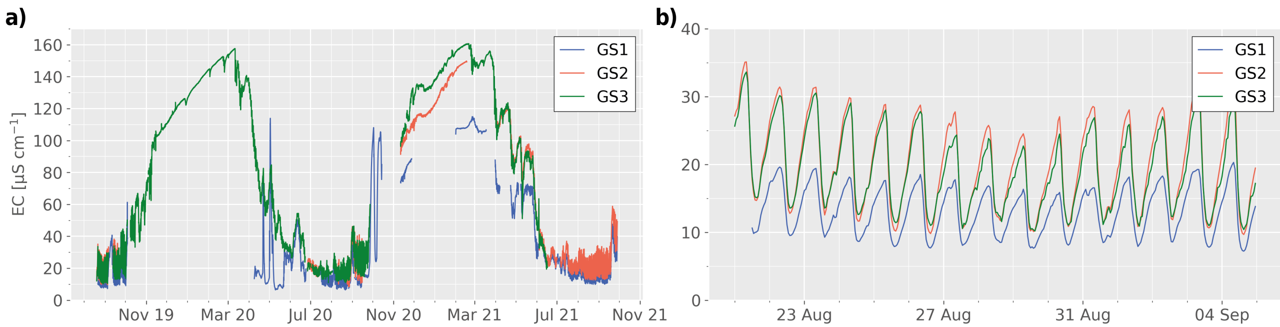


**Figure 4. a)** Streamflow electrical conductivity (EC) at the three gauging stations (GS1 to GS3, see Fig. 2) during two years. **b)** Zoom-in window showing the EC for the first 20 days of measurement. Large gaps in winters are due to sensor failures.

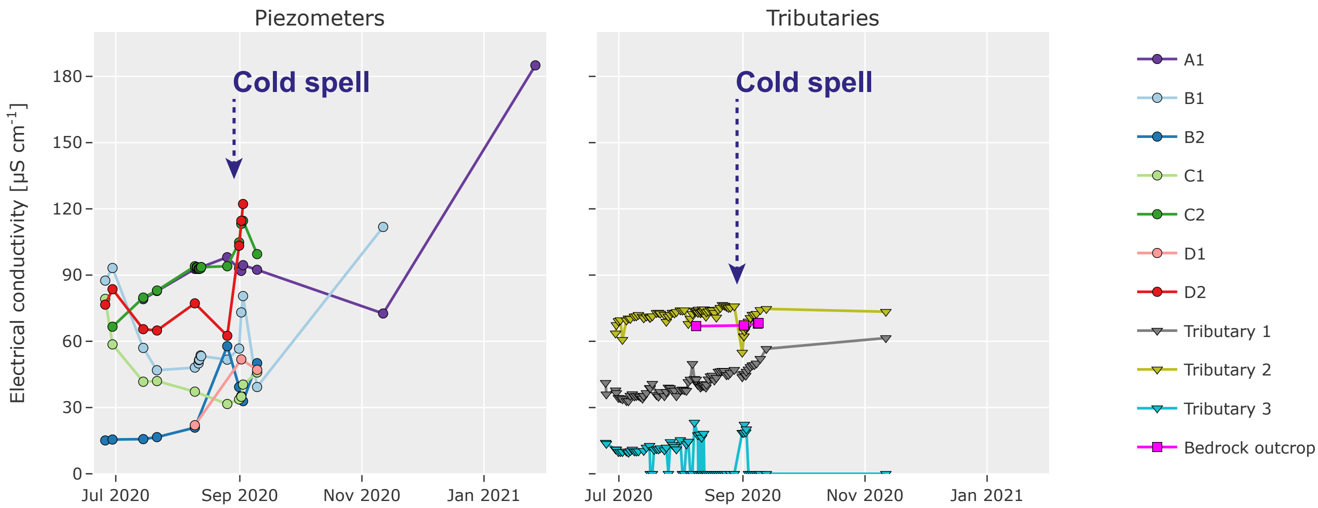


**Figure 5.** Temporal evolution of EC at seven wells (A1 to D2) in the outwash plain, in three tributaries as well as one bedrock spring (see Fig. 2 for location). Values of 0 for tributary 3 indicates no surface flow. A cold spell resulting in snow fall over the whole catchment is indicated by the dark blue arrow.

sediments of the lateral moraine and re-emerges at the base of the outwash plain. During a cold spell (August 30), accompanied by a heavy rain event (42 mm) on the preceding day, a small drop in EC in tributary 2 can be observed and is likely related to an increased water storage in the lateral moraines, which empties in a few days. Tributary 3 maintains low EC close to the value of snowmelt and becomes dry in August, indicating its direct dependence on snowmelt transmitted by overland flow with hardly any contact time with the sediments.

The EC measured in the groundwater wells show much stronger variations, both spatially and temporally (Fig. 5). In the upper part of the outwash plain (wells $B$, $C$, $D$), EC is low near the stream, indicating strong stream water-groundwater exchanges. Near the hillslopes, EC is higher and also larger than the tributaries, indicating either contribution from deeper hillslope exfiltrations with higher EC or river contribution with long flowpaths from the stream network. During the cold spell, river discharge decreased and groundwater EC became larger in C2 and D2 likely due a decreased infiltration from the river and an increased influence from a deeper groundwater source. Well A1 shows a smoother signal, with high values year-round and a gradual increase in summer, likely due to the decreasing snowmelt contribution in the outwash plain. During winter, groundwater EC in well A1 increases rapidly reaching 180 $\mu S/cm$.

## 4.2 Groundwater dynamics in the outwash plain

From the groundwater head observations in the outwash plain, we computed the daily averaged lateral (perpendicular to the stream) and longitudinal (parallel to the stream) aquifer gradients (Fig. 6). During the summer the lateral upstream gradient (well D1-D2) is mostly comprised between 0 and 0.5%. The EC at well D2 is similar to tributary 2, which suggests a hillslope recharge from tributary 2, or a constant deeper bedrock exfiltration which maintains a mild lateral gradient towards the stream. The lateral downstream gradient (well B1-B2) shows a stronger slope of about 1% in the direction of the stream, which gradually decreases to values close to 0% by September. This gradient seems closely related to the snowmelt fed tributary 3. Indeed, well B2 shows a low EC in the early melt season, similar to tributary 3, which only increases in mid-August when this tributary runs dry (Fig. 5).

The longitudinal gradient seems to maintain a larger slope of about 1 to 2% during the summer. Interestingly, the daily discharge in 2020 shows a similar weekly dynamic to the upstream gradient, although the gradient tends to react with a delay of 1 to 2 days. This suggests a strong influence of the stream discharge magnitude on the upstream gradient, which starts decreasing only in early September, i.e. at the moment when discharge peaks decrease.

River stages corresponding to the well transects could not be measured continuously due to the high discharge and unstable sediments; a few isolated measurements show that, in the upper part of the floodplain (B, C, D transects), the river stage is always 10 to 40 cm higher than the groundwater level close to the river, indicating a lateral gradient in the opposite direction from the stream to the well close to the river, and thus a loosing stream reach. Higher discharge therefore leads to higher river stage, which increases the hydraulic gradient through the riverbed and therefore promotes higher infiltration.

Based on the hydraulic gradients, it appears that groundwater flows in the same direction as the terrain's main slope, is recharged in its upstream part by the stream and re-emerges at the end of the outwash plain. This re-emergence results from the underlying bedrock with much lower hydraulic conductivity, which forces water to exfiltrate in the river as the sediment thickness decreases towards the end of the plain. This groundwater upwelling is also supported by the EC in well A1 (Fig. 5) which shows the highest EC in the floodplain, although it is located at 5 m from the river, indicating long flowpaths and no direct contact with the river at this location.

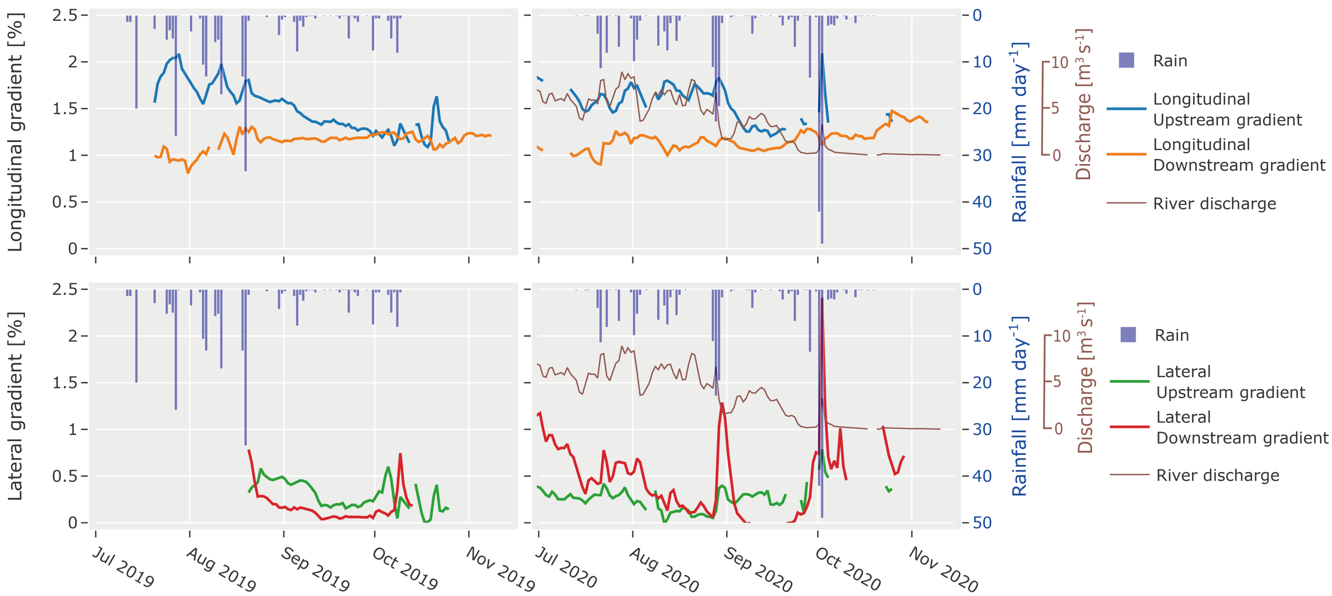


**Figure 6.** Groundwater gradients in the outwash plain for summers 2019 and 2020. The upstream longitudinal gradients are estimated between wells D1 and C1, the downstream gradient between C1 and B1. The lateral gradients are estimated between *D* wells upstream and *B* wells downstream and their slope is directed towards the main river. In 2020, the mean daily discharge at the glacier outlet (GS1) is shown in brown and was scaled between 1 and 2% slope for easier comparison with the gradients. Daily measured rainfall at the glacier snout (weather station) are shown by inverted blue bars.

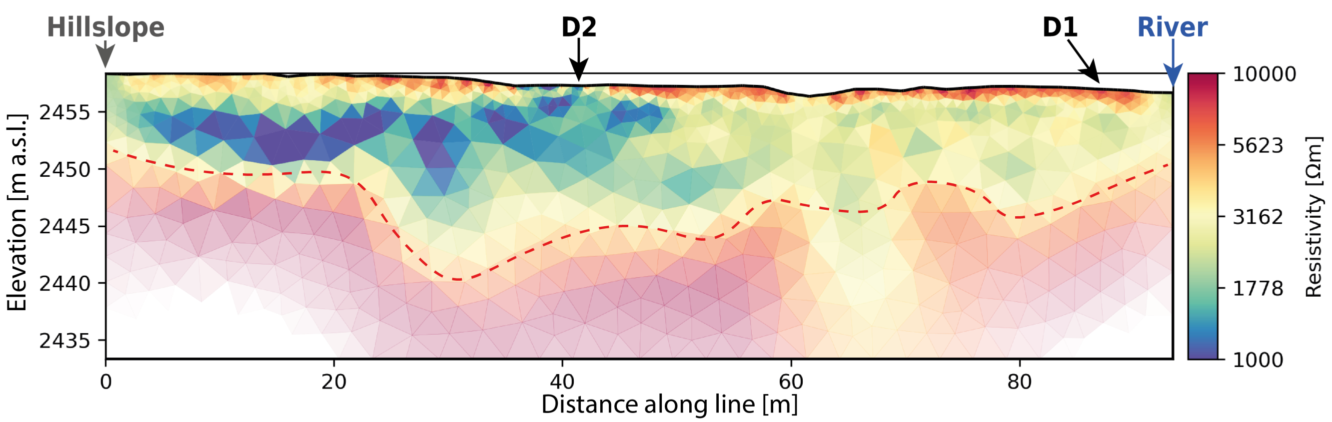


**Figure 7.** Results of ERT profile perpendicular to the stream at location of groundwater wells D1 and D2. Electrode arrays consists of 48 electrodes with 2m spacing. Robust inversion was performed for the Dipole-Dipole scheme using a regularization coefficient lambda of 10. Location of groundwater wells as well as the hillslope and river sides are also highlighted. The red dashed line shows the limit between water-filled sediment and underlying bedrock.

### 4.3 Hydraulic conductivity in the outwash plain

#### 4.3.1 Pressure wave diffusion

We identified aquifer thickness using ERT and illustrate the results for well transect D1-D2 (Fig. 7). A thin layer of dry sediments can identified at the top, following a lower layer where resistivity is in a range between 1000 and 3000 $\Omega$ m$^{-1}$. Near the stream, resistivity is slightly higher, likely due to lower groundwater EC close to the stream than the hillslope. The bedrock is located at a depth of about 10 to 15 meters with resistivity higher than 5000 $\Omega$ m$^{-1}$.

Using the diffusion model (Sect. 3.1), we modeled the diffusion of stream stage fluctuations in the aquifer, estimated diffusivity and obtained hydraulic conductivity using an aquifer thickness (15 meters) and porosity, with an average value of 0.25. Unlike in the work of Magnusson et al. (2014), satisfying results were obtained using a unique $K_s$ value to simulate the fluctuations of all wells along the same transects (Fig. A1 and A2). The results are summarized in Table 1. Only the estimated lower value for the well transect *D* in September 2019 appears more uncertain, as the simulated head variations for well D1 at 5 m from the river do not match well the observed results (Fig. A2b).

| | High flow $K_s$ [m s$^{-1}$] | Low flow $K_s$ [m s$^{-1}$] |
|---|---|---|
| Upstream transect (D1 and D2) | $2.5\times10^{-3}$ | $0.96\times10^{-3}$ |
| Downstream transect (B1, B2 and B3) | $7.6\times10^{-3}$ | $5.6\times10^{-3}$ |

**Table 1.** Estimated saturated hydraulic conductivity of the outwash plain for high flow and low flow conditions during the summer period along two transects based on the pressure wave diffusion model.

#### 4.3.2 Salt tracer injection

The passage of the salt plume was identified by a change of resistivity (of more than an order of magnitude) in a well constrained zone of the ERT line (plume radius of about 1 m), with the maximum change occurring 10.5 to 11.5 hours after injection. Using a travel distance of 9.38 m, we obtain an average pore velocity $v_p$ of $2.4\times10^{-4}$ m s$^{-1}$. The corresponding aquifer gradient between 3 groundwater wells (one 1 m upstream of the injection point and two along the ERT line) has a maximum slope of 1.7%. Based on these values, we obtain an estimated hydraulic conductivity of $3.5\times10^{-3}$ m s$^{-1}$. A detailed illustration of the timelapse ERT is available on Zenodo (Müller, 2022c). The surface hydraulic conductivity estimated with this second approach leads to an estimation of the hydraulic conductivity close to the mean of the values estimated with the diffusion model ($4.2\times10^{-3}$ m s$^{-1}$).

| Author | Landform | Method | Aquifer slope [%] | Porostiy [-] | Aquifer length [m] | Slope parameter b [-] | Reported Ks [m s^-1] | | Reported recession constant 1/α in study [days] | Calculated recession constant 1/α [days] | |
|---|---|---|---|---|---|---|---|---|---|---|---|
| | | | | | | | min. | max. | | min. | max. |
| Clow et al. (2003) | **Talus slopes** | Recession analysis | 25 | 0.30 | 200 | 1 | 6.50E-03 | 9.40E-03 | - | 0.3 | 0.4 |
| Caballero et al. (2002) | **Talus slopes** | Kinematic wave propagation | 25 | 0.30 | 200 | 1 | 6.90E-04 | 2.50E-03 | - | 1.1 | 4.1 |
| Muir et al. (2011) | **Talus slopes** | Wave + tracer (chloride) | 25 | 0.30 | 200 | 1 | 1.00E-02 | 3.00E-02 | 1 | 0.1 | 0.3 |
| Kurylyk et al. (2017) | **Talus slopes** | Kinematic wave propagation | 25 | 0.30 | 200 | 1 | 2.00E-03 | 2.00E-02 | - | 0.1 | 1.4 |
| Caballero et al. (2002) | **Lateral glacial deposits** | Kinematic wave propagation | 25 | 0.25 | 200 | 1 | 2.90E-04 | | - | 8 | |
| Rogger et al. (2017) | **Lateral glacial deposits** | Grain size analysis | 25 | 0.25 | 200 | 1 | 2.22E-04 | | - | 11 | |
| Langston et al. (2013) | **Glacial deposits** | Mass balance | 8 | 0.25 | 1000 | 1.5 | 3.00E-04 | 3.00E-03 | - | 12 | 121 |
| Magnusson et al. (2012) | **Glacial deposits** | Slug test | 8 | 0.25 | 1000 | 1.5 | 6.94E-05 | 4.86E-04 | - | 74 | 521 |
| Kobierska et al. (2015) | **Glacial deposits** | Tracer propagation (salt) | 8 | 0.25 | 1000 | 1.5 | 5.15E-04 | 1.35E-03 | 0.27 (fast resevoir)<br>29 (slow reservoir) | 27 | 70 |
| Winkler et al. (2015) | **Rock glacier** | Tracer propagation (fluorecent) | 15 | 0.30 | 500 | 1 | 7.00E-05 | 4.60E-02 | 21 (early recession)<br>125 (20-80 days)<br>500 (late recession) | 0.3 | 167 |
| Rogger et al. (2017) | **Rock glacier** | Grain size analysis | 15 | 0.30 | 500 | 1 | 5.56E-03 | | - | 2 | |
| Harrington et al. (2018) | **Rock glacier (summer melt)** | Kinematic wave propagation | 15 | 0.30 | 200 | 1 | 5.00E-03 | 1.00E-02 | 3 to 4 | 0.5 | 1 |
| Harrington et al. (2018) | **Rock glacier (baseflow)** | Spring discharge (Darcy) | 15 | 0.30 | 200 | 1 | 6.00E-05 | 2.00E-04 | 14 to 50 | 23 | 78 |
| Robinson et al. (2008) | **Outwash plain (sandur)** | Grain size analysis | 2 | 0.25 | 1000 | 1.5 | 1.16E-04 | 1.74E-03 | - | 83 | 1250 |
| Ó Dochartaigh et al. (2019) | **Outwash plain (sandur)** | Pumping tests | 2 | 0.25 | 1000 | 1.5 | 2.89E-04 | 4.63E-04 | - | 313 | 500 |
| Käser et al. (2016) | **Outwash plain** | Pumping test | 2 | 0.25 | 1000 | 1.5 | 6.00E-04 | 5.00E-03 | - | 29 | 241 |
| This study | **Outwash plain** | Pressure wave diffusion | 2 | 0.25 | 1000 | 1.5 | 9.60E-04 | 7.60E-03 | - | 19 | 151 |

**Table 2.** Calculation of the recession constant $1/\alpha$ for different landforms based on typical aquifer structure ($h_L/L$, $\phi$ and $L$) and a review of hydraulic conductivity ($K_s$) reported in proglacial studies. Maximum and minimum values of $K_s$ are given where applicable. Values of $1/\alpha$ for studies which estimated this parameter based on discharge recession analysis, independently from $K_s$ were also reported.

## 4.4 Landform-based groundwater storage dynamics

In order to disentangle the relative contribution of different superficial landforms, we propose to compare the recession constant ($1/\alpha$), which provides a way to compare how fast each aquifer compartment releases water and what is their significance to maintain flow during dry periods. We reviewed studies focusing on specific landforms in glaciated catchments where hydraulic conductivity ($K_s$) was estimated in Table 2.

We then estimated the storage and response time of each unit in the Otemma catchment using the landform-based model (Sect. 3.5) based on $K_s$ values from Table 2, including maximum and minimal $K_s$ values to account for uncertainty. We also defined aquifer properties realistic for our catchment (Table 3). For lateral moraines (Caballero et al., 2002; Rogger et al.,

| | Landform area ($A_i$) [km$^2$] | Slope [°] | Porostiy [-] | Aquifer length [m] | $c$ [-] | $K_s$ [m s$^{-1}$] min. | mean | max. | $1/\alpha$ [days] min. | mean | max. |
|---|---|---|---|---|---|---|---|---|---|---|---|
| Talus slope | 1.58 | 27 | 0.30 | 250 | 1 | 7E-4 | 2E-3 | 1E-2 | 0.19 | 1 | 2.8 |
| Lateral moraine | 4.99 | 27 | 0.25 | 250 | 1 | 1E-4 | 3E-4 | 5E-4 | 3.2 | 5.4 | 16.2 |
| Glacial deposits | 2.16 | 10 | 0.25 | 500 | 0.5 | 3E-4 | 6.5E-4 | 1E-3 | 8.6 | 13.3 | 28.8 |
| Outwash plain | 0.14 | 1.15 | 0.25 | 1000 | 0.5 | 1E-3 | 4E-3 | 7E-3 | 20.7 | 36.2 | 144.7 |

**Table 3.** Estimated recession constant ($1/\alpha$) based on aquifer characteristics of the entire Otemma catchment for the main landform compartments. $c$ stands for the slope coefficient of Eq. 4 and was defined to be 1 when aquifer slope is larger than 10°.

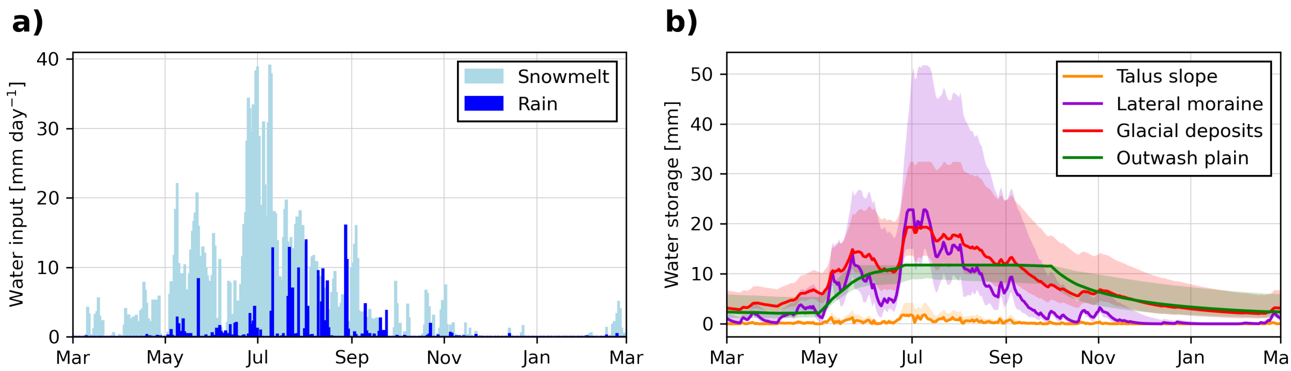


**Figure 8.** a) Measured precipitation input at glacier snout [mm day$^{-1}$] and mean snowmelt input simulated with the simple degree day approach [mm day$^{-1}$]. b) Evolution of the groundwater storage of the four main geomorphological landforms (outwash plain; flat glacial deposits <22°; lateral moraines >22°; talus slopes >22°) based on the landform-based model described in Eq. 12 to 14. Storage volumes in m$^3$ are divided by the entire catchment area in m$^2$ to provide comparable estimates in mm.

2017), we selected $K_s$ to be smaller than for flatter deposits (Kobierska et al., 2015a), which probably reflects the lesser degree of compaction at the valley bottom. We separated talus slopes from lateral moraine as talus slopes material is coarser and lay above the LIA line. For the outwash plain, we used our own estimate of the hydraulic conductivity and for mildly sloping glacial deposits, comprised between a slope of 8 to 22°, we used a mean slope of 10° as the majority of those deposits were rather flat.

Supported by a simple degree-day model for snow accumulation and melt, we estimated the catchment-scale average rainfall and snowmelt during the year 2020. Rainfall amounts to a total of 204 mm and snowmelt to 1732 mm of water equivalent (see Fig. 8a). Figure 8b shows the resulting estimated maximum storage for each landform.

The resulting maximum baseflow storage in the flat glacial deposits is 19 mm (with an uncertainty margin from 13.5 to 32.5 mm) or a maximum aquifer thickness of 1.1 m (0.8 to 1.8 m) during peak snowmelt. The storage in the outwash plain gradually increases due to constant recharge from the river and rapidly reaches its maximum storage of 11.3 mm (or an aquifer

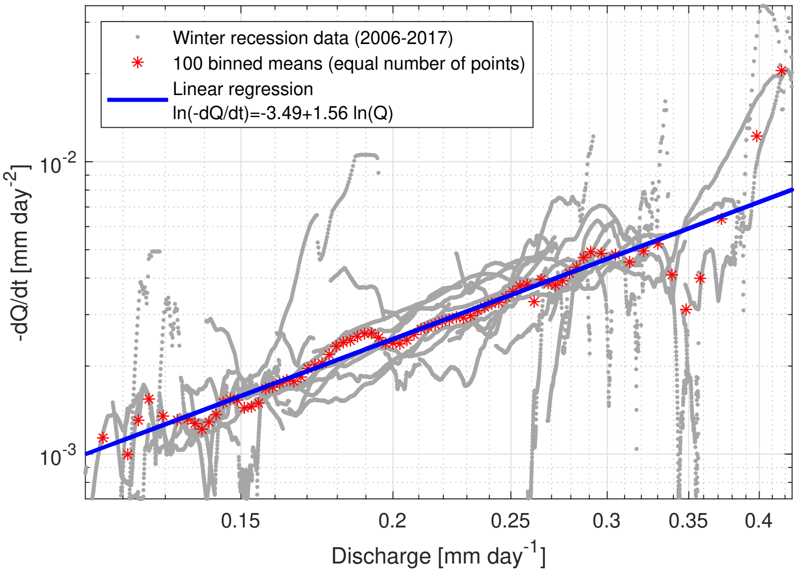


**Figure 9.** Plot of the smoothed discharge recessions ($-dQ/dt$) against discharge ($Q$) for all recession periods from 2006 to 2017 (in grey) at the catchment outlet (GS3). Binned averages are shown in red, each bin comprising 1% of the datapoints. A linear regression (in the logarithmic space) to all binned values smaller than 0.33 mm day$^{-1}$ is plotted in blue. Axes are in logarithmic scale.

thickness of 10 m). The lateral moraines show a very flashy storage response linked to their short recession constant. Their storage reaches 23 mm (15 to 52 mm) during snowmelt, corresponding to an aquifer thickness of 0.55 m (0.35 to 1.25 m). Due to their very low retention capacity, talus slopes only transmit water and their storage is low with only 1.8 mm (1 to 4.5 mm) and a maximum aquifer thickness of 0.11 m (0.06 to 0.27 m). After peak snowmelt, storage decreases quickly in the lateral moraines and somewhat slower in the flatter glacial deposits, while maximum storage is maintained in the outwash plain due to the stream recharge. During autumn, lower discharge leads to a storage decrease in the outwash plain too, so that by early December the total remaining storage becomes very limited with only 8.8 mm (5 to 20 mm) remaining from the outwash plain and flat moraine deposits.

### 4.5 Catchment-scale winter river recession analysis

Discharge recession was analyzed from 2006 to 2017 at the catchment outlet by calculating the averaged relationship between recession rates ($dQ/dt$) and river discharge ($Q$) (Fig. 9). A change of slope occurs for discharge higher than 0.33 mm day$^{-1}$, probably due to the transition between discharge dominated by ice melt to discharge fed by groundwater. Due to this slope change, we assume that the recession starts when baseflow discharge is smaller than 0.33 mm day$^{-1}$ and higher values are excluded for the linear regression shown in Fig. 9.

The estimated regression has a slope of $b$=1.56, leading to a quadratic relationship between storage and discharge (Eq. 6). Due to the low values computed in Fig. 9, a change in the smoothing process of the raw discharge data may have an impact

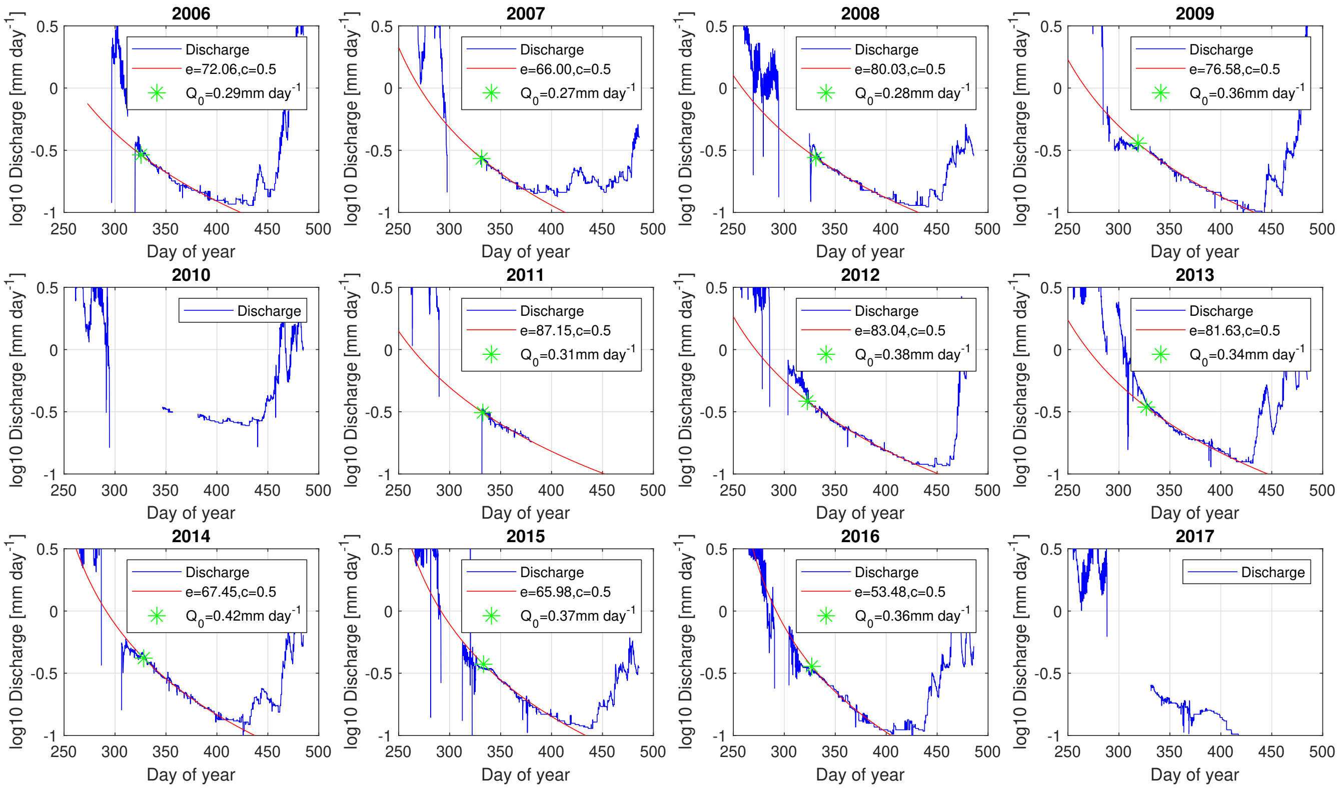


**Figure 10.** Annual recession analysis at the catchment outlet (GS3). The measured discharge is presented in blue (logarithmic scale), the best fit of the power-law regression ($Q_t = Q_0(1 + \frac{1}{e}Q_0^{0.5}t)^{-2}$) is shown in red, along with the estimated fitted parameters $Q_0$ and $e$. Day of year larger than 365 indicates a recession spanning over the following year. The years 2010 and 2017 have large data gaps and are not shown.

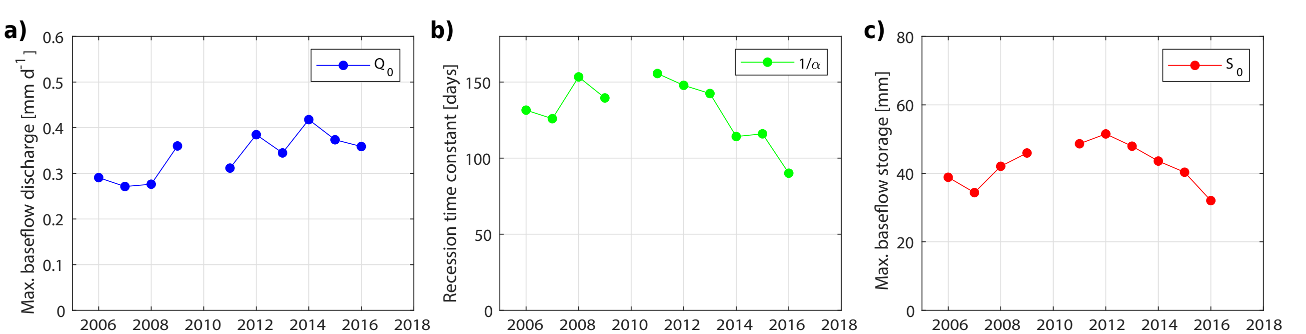


**Figure 11.** Temporal evolution of recession characteristics obtained from annual recession analysis of Otemma catchment, showing the results of the best fitted parameters for **a)** maximum baseflow ($Q_0$), **b)** recession constant ($1/\alpha$) and **c)** maximum baseflow storage ($S_0$).

on the recession. We have tested different processing parameters and assessed the impact on the linear regression; overall, the slope varies between 1.45 and 1.65.

Using the same recession periods, the recession trends of each individual year is assessed (Fig. 10) using a quadratic relationship (Eq. 8) and fitting the maximum baseflow discharge ($Q_0$) and the recession coefficient ($e$). The corresponding calculated recession constant ($1/\alpha$) seems to decrease in the recent years but the trend is unclear due to the overall short time period, while the temporal evolution of $Q_0$ and $S_0$ does not show any trend, suggesting no clear increase in groundwater storage over the twelve years period (Fig. 11).

Overall, we obtain a similar estimation of the baseflow storage in the Otemma catchment during each winter, with a mean maximum baseflow discharge of 0.34 mm day$^{-1}$, a mean maximum storage of 42.5 mm and a recession constant ($1/\alpha$) comprised between 90 and 155 days. Finally, at the end of the recession periods in late winter, discharge has decreased by a factor of 3 which indicates that the baseflow storage does not completely empty and still retains on average 58% of the maximum baseflow storage of early December.

Those results are in contradiction with the landform-based model (Fig. 8), where a maximum baseflow storage during early December was estimated to only 8.5 mm. Accordingly, the landform-based analysis seems to miss a relatively important storage compartment.

# 5 Discussion

## 5.1 Groundwater storage and release functions of the main geomorphological features

Our analysis has shown that the landform- as well as the catchment-scale hydrological response critically depends on i) the sediment structure defining $K_s$ and ii) the landform characteristics in terms of slope and aquifer flow paths length. These key properties can then be combined to estimate an averaged response time of each landform, although the storage-release behavior may be more complicated when considering more complex aquifer geometries (Berne et al., 2005), heterogeneous landforms with varying physical propriety for $K_s$ and $\phi$, preferential flow paths (Harman et al., 2009) or non-stationary processes (Benettin et al., 2017). In this study, we focused on characterizing the "slow" groundwater compartment which is relevant for baseflow only, but an initial part of the water release may also occur in a faster superficial layer, as suggested in other studies (e.g. Winkler et al., 2016; Kobierska et al., 2015b; Stewart, 2015). Our approach, while simple, relies on physical properties of the aquifer. The calculated values for 1/$\alpha$ were similar to studies which estimated this parameter based on direct observations of discharge recession. This supports the validity of our approach to analyze the storage-release behavior and the relative importance of different landform units in a glaciated catchment.

With this analysis, we have shown that only flat aquifers release water at time scales longer than weeks. In addition to $K_s$, the bedrock slope plays an important role, as it changes the relationship between storage and discharge, illustrated in our landform-based model by the slope coefficient $c$. Indeed, steeper slopes promote stronger advective fluxes (Harman and Sivapalan, 2009a) and modify the recession equation (Eqs. 7 and 10), so that a sloping aquifer ($c$=1) would loose 50% of its storage 1.4 times faster and 99% 4.5 times faster than a flat aquifer ($c$=0.5).

The seasonal landform-based analysis of superficial storage proposes an example of the groundwater dynamics in a glaciated catchment. The estimated storage amounts are likely not accurate due to a strong simplification of the recharge processes and the absence of superficial overland flow; it nevertheless illustrates i) the strong relationship between recharge and storage, ii) the importance of the timing of the water input and iii) the relative speed at which different reservoirs may empty. Accordingly, we can establish a sound perceptual model (see Sect. 5.3).

Prior to introducing this model, we first discuss and summarize hereafter what new insights we gain from our case study on the hydrological functioning of the main classes of geomorphological landforms.

### 5.1.1 Talus slopes

In the Otemma catchment, talus slopes have only a marginal extent so that the estimated storage is very low. In other less glaciated catchments, talus slopes may cover a much larger area, but, due to their coarse aquifer structure, their recession constant is only of the order of a day (Table 2), leading to a rapid transmission of water and little storage capacity. This is illustrated in our landform-based model by a maximal aquifer thickness of 11 cm. Therefore, groundwater storage is likely discontinuous and may only occur in pockets due to bedrock depressions at the base of the talus (fill and spill mechanism (Tromp-Van Meerveld and McDonnell, 2006; Muir et al., 2011)). If a less conductive layer exists at the bottom of the talus, most studies have only reported a few centimeters of water saturation with relatively high conductivity (Muir et al., 2011; Kurylyk and Hayashi, 2017). Some studies have however shown different results, mainly the study by Clow et al. (2003), who estimated an aquifer thickness of a few meters and concluded that talus slopes contributed up to 75% of winter baseflow. We want to stress here that this study is based on an erroneous calculation of the storage-discharge relationship where the authors wrongly included the time. This mistake may have influenced the conclusions made by others and we insist here that talus slopes do not have the capacity to store water; they only transmit it from and to other landforms or the underlying fractured bedrock as also suggested by others (e.g. McClymont et al., 2011; Harrington et al., 2018).

### 5.1.2 Steep lateral moraines

Steep lateral moraines may present glacial deposits of the order of tens of meters (Rogger et al., 2017) and have a lower hydraulic conductivity than talus slopes. Even though their structure is steep, they may retain water at a time scale of around one week. Their response remains relatively flashy and the amount of potential storage is mainly driven by the rate of snowmelt in the early summer season. This is illustrated in our field observations in early September 2020, where the EC in Tributary 2 recovers rapidly after a heavy rain event (Fig. 5) and where the lateral downstream gradient decreases on the same time scale (Fig. 6). Additionally, EC difference between the bedrock outcrop and Tributary 2 is marginal, indicating limited chemical weathering and thus fast subsurface flow.

In our landform-based model, we assumed an homogeneous recharge, which is unlikely in the late mid-summer season, when snowmelt mainly occurs in the upper part of the catchment or in hanging valleys, and when both surface and subsurface melt water responsible for its recharge are likely concentrated in gullies or other zones of flow convergence due to the bedrock topography. The amount of recharge of steep lateral moraines is thus likely dependent on the frequency of flow convergence upslope; the more concentrated is the upslope flow, the less recharge occurs. In Otemma, these concentrated flows seem rather superficial with limited infiltration into deeper parts of the moraine, which is likely due to more cemented grains and early soil development, and thus further limits recharge. Part of the water does nonetheless infiltrate and re-emerge at the foot of the hillslope as in Tributary 2. Thus, the estimated storage of such landforms due to snowmelt is likely not as large as estimated here (23 mm), as only a fraction of this landform is located above zones of snowmelt induced recharge. They have however the potential to store significant amounts of rain water, at least in the Otemma catchment, as they cover a significant part of the whole catchment (about 20%). Finally, as suggested in other mountainous areas (Baraer et al., 2015), it is also possible that some water may reach the bottom of the moraine with lower hydraulic conductivity and directly exfiltrates into the outwash plain underground, making direct observations not possible. This phenomenon may explain the increase in EC observed in well C2 and D2 during the cold spell, which is likely due to older groundwater from the slopes (Fig. 5). Based on our landform-based model, such groundwater flow should still be relatively fast due to the steep slopes so that this older water may also come from bedrock exfiltrations transmitted through the moraine to the outwash plain.

#### 5.1.3 Flatter glacial deposits

Flatter glacial deposits, such as alluvial fans or melt-out till moraines have a similar structure to steeper moraines but are usually less cemented and may present an eluviation of fine sediments, leading to a somewhat greater hydraulic conductivity (Langston et al., 2011; Ballantyne, 2002). In Otemma, those mildly sloping structures are dominated by moraine deposits and their recession constant was estimated to be 2 to 3 times larger than for steeper moraines. Their water release is also slower due to a weaker advective flux and more diffusion, which we illustrated using a quadratic form of recession ($c$=0.5, see Eq. 6). An aquifer slope of 10° is however at the upper limit of such a recession equation, so that the actual drainage is probably faster, more similar to steeper lateral moraines. Their capacity to sustain baseflow depends on the amount and timing of water recharge during the snowmelt period. Where glacial deposits are connected to a more constant source of water such as ice melt, storage may remain high throughout the summer (Kobierska et al., 2015b), and they will function similarly to an outwash plain as described hereafter. In the case of the Otemma catchment, the usual thickness of these sediments is on the order of tens of meters, making direct groundwater observation at their base not possible. No clear changes in EC was observed in summer beyond the outwash plain (between GS2 and GS3), a section where morainic material is present, which could indicate a marginal contribution from this area, but the signal is likely dampened by additional ice-melt with low EC from hanging glaciers. In winter, a slight increase between GS2 and GS3 is observed, suggesting some groundwater contributions, which could be attributed to the morainic deposits or bedrock exfiltration.

#### 5.1.4 Outwash plains

Outwash plains show strong surface water-groundwater interactions, which maintain near saturation conditions far after the peak of snowmelt as long as glacier melt maintains stream discharge. Our field observations show that stream infiltration is the main source of recharge in the upstream part and reaches far from the stream in summer, as illustrated by the higher EC near the hillslope and in the well A1 near the lower end of the plain. This was previously shown by others (Mackay et al., 2020; Ward et al., 1999).

In winter, groundwater EC increases largely in A1, but this increase is also partially due to an increase of EC in the source water, i.e. the upstream river with similar EC values to GS1. In fact, the difference in EC between A1 and the stream at GS1 does not change much between summer (about 70 $\mu S/cm$) and winter (about 80 $\mu S/cm$), which indicates a strong connection year-round, a limited change in EC with depth in the aquifer and a groundwater transit time which only increases slightly in winter. Nonetheless, the EC difference in the stream before (GS1) and after the outwash plain (GS2) increases in winter, indicating that the outwash plain seems to contribute to some extent to baseflow, but also that an upstream groundwater source above GS1 drives the EC increase in the stream before it enters the outwash plain.

Our landform-based model, based on our estimation of $K_s$, validates these observations, as it was shown that the outwash plain provides some baseflow in winter due to its longer recession constant (about 35 days). Compared to older alluvial systems (Käser and Hunkeler, 2016; Ó Dochartaigh et al., 2019), our estimates of $K_s$ are slightly larger maybe due to a less consolidated aquifer and the absence of vegetation. If the current role of outwash plains in maintaining baseflow is clearly limited due to their small areal extent in alpine catchments, future glacier retreat may extend their area, especially where bedrock overdeepenings can be filled with sediments. Finally, together with earlier snowmelt in a warming climate, their role in providing baseflow during drought conditions is likely to become increasingly important in the future.

#### 5.1.5 Missing storage

From the above comments and the landform-based model (Fig. 8), it appears that the current capacity of the superficial geomorphological landforms to store water is limited to the melt period, with the exception of the outwash plain and maybe some flatter glacial deposits, with only about 8.5 mm of storage remaining in early December (i.e. at the start of the winter recession). Nonetheless, on the basis of baseflow recession analysis at the catchment-scale, we estimated a potential groundwater storage of the order of 40 mm. This value was estimated using a simple mathematical relationship between storage and discharge, which has been shown to be sensitive to the choice of the recession periods, which may include processes which are not directly linked to aquifer drainage (Staudinger et al., 2017). For instance, in our study, the recession analysis may be biased if substantial basal ice-melt provides water during winter, which we cannot exclude. Nevertheless, even if the estimated value may not fully represent the real storage in the catchment, the catchment-scale recession time scales of about 100 days cannot be explained by the superficial landforms present in the catchment, and stream EC at the glacier outlet (GS1) does show a strong increase in winter, supporting the presence of an unidentified compartment, which was not included in the landform-based model. Finally, the measured cumulated winter discharge (December to end of March) at GS3 is in the order of 20 to 25 mm each year, further supporting the presence of a missing storage compartment, which slowly drains during the whole winter.

We propose here some hypotheses concerning its nature. The first hypothesis is that the remaining baseflow recession in winter is actually not due to a storage unit, but rather to some residual snowmelt or permafrost losses or due to basal melt at the glacier bed. Snowmelt and permafrost losses are not very likely during the cold season as mean air temperature at the weather station is around -5 to -10°C. Basal melt may however occur during the whole winter due to the overburden pressure of the ice-mass (Flowers, 2015). The second hypothesis is the contribution from a groundwater reservoir underneath the glacier itself which is recharged in summer, without winter basal ice melt. Previous studies have however predicted a rather rocky or

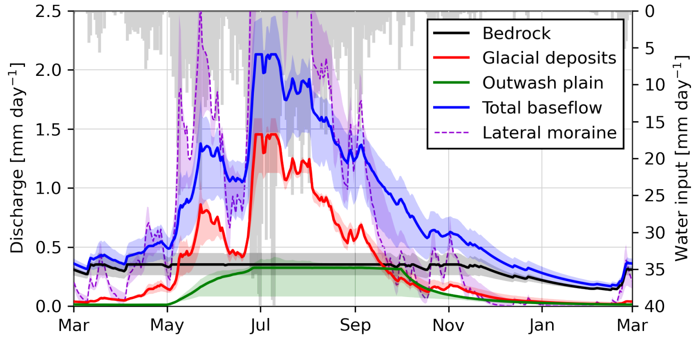


**Figure 12.** Evolution of modelled groundwater baseflow discharge of different hydrogeomorphological landforms. Total baseflow represents the sum of outwash plain, moraines and bedrock discharge; steep lateral moraines are also plotted but are not considered into the sum of baseflow due to their fast response. Simulated total water input (snowmelt and rain) are plotted in grey.

mixed glacial bed in this area (Maisch et al., 1999), with limited till thickness on the order of tens of centimeters and with a likely discontinued nature (Harbor, 1997). A large enough reservoir (four times the current outwash plain) could exist in a large glacial overdeepening but it is unclear if sufficient sediments would accumulate in such a pocket based on the sediment export capacity of the glacier. The smooth increase in EC at GS1 during winter, could better be explained by a combination of the first two hypotheses were a smaller subglacial reservoir is recharged by decreasing basal melt which slowly empties during winter and acquires solutes by the weathering of bedrock or sediment.

The third hypothesis is that the storage occurs mainly in the bedrock and that sufficiently short flowpaths allow this storage to drain during the winter. This hypothesis is likely since large fractures may occur due to glacier debuttressing (Bovis, 1990; Grämiger et al., 2017) and groundwater seepage through deep fractures probably occurs underneath other landforms and cannot be identified clearly. Moreover, some studies have reported similar catchment-scale storage in elevated catchments, although it is usually not clearly associated with a distinct hydrological unit. In particular, in a similar highly glaciated catchment, the work of Hood and Hayashi (2015) reported a peak catchment-scale storage in spring of 60 to 100 mm. Moreover, the work of Oestreicher et al. (2021) modelled an estimated catchment-scale storage change of 70 mm in a Swiss glaciated catchment of similar glacier coverage, which they could relate to a deep borehole water head change (Hugentobler et al., 2020). Such estimates represent the peak spring storage, accounting for all storage units, and not only the winter storage estimated in our study. Based on the rough estimates of Fig. 8, the peak summer storage estimated is 30 mm for flat glacial deposits and the outwash plain and 23 mm for the steep lateral moraines, which, combined with a bedrock storage of 40 mm, would result in similar numbers. Finally, during a cold spell in Otemma, some evidence of the contribution of deeper, older groundwater was observed as depicted by a fast increase in EC in well C1 and D1, which could also be due to older water exfiltrating from the bedrock.

Based on the above discussion, we propose to allocate the missing storage to bedrock storage with a maximum of 40 mm, which we can then add to our previous landform-based model (Eq. 12) with a recession constant ($1/\alpha$) of 115 days to reflect the baseflow recession analysis. The resulting baseflow of each landform is shown in Fig. 12.

### 5.2 Landform hydrological connectivity

While our approach identifies the relative size and seasonal hydrological response of proglacial landforms, we use a simplistic recharge model. In reality, hydrological connectivity from the water sources and between landforms will ultimately drive the amount of actual recharge. Due to the coarse and barren nature of the sediments in proglacial landforms and the limited presence of soils, it can be expected that any water input infiltrates into the sediments (Maier et al., 2021). It has also been shown that groundwater flow is driven by the bedrock topography underneath the landform, where a strong change in hydraulic conductivity drives the water downslope (Hayashi, 2020; Vincent et al., 2019). We can therefore assume that recharge occurs directly at the location of the water input, percolates until the bedrock and is then directed downslope. In the case of snowmelt, this recharge will gradually move upslope as snow melts during the summer, a zone where talus slopes and bedrock are frequent. Water will rapidly be directed downslope at the bedrock interface and directed in zones of bedrock depression, concentrating the flow as discussed in Sect. 5.1.2, and thus providing little recharge to other downhill sloping deposits. Water may also reach a flatter zone in hanging valleys, where flatter morainic material may be present in rock overdeepenings, which likely act as an immobile storage, where groundwater only overflows above the bedrock similarly to a fill and spill mechanism (Tromp-Van Meerveld and McDonnell, 2006). The concentrated groundwater flow eventually reaches either the main stream or a flat glacial deposit (moraine or outwash plain) and acts as point recharge, so that only areas located below a zone of bedrock convergence will receive recharge. Similarly, glacier melt recharge will mostly occur along the reach of the glacial stream at the valley bottom and will maintain high groundwater storage in outwash plains or flat moraines exclusively.

### 5.3 A sound perceptual model for the hydrological functioning of a glaciated catchment

We summarize here the gained insights into a perceptual model (Fig. 13) of the hydrological functioning of the Otemma catchment, augmented with an additional "missing" storage which we tentatively allocate to bedrock (Sect. 5.1.5). In this representation, the partitioning between the different sources of water recharging each landform are taken from the result of our landform-based model of the Otemma catchment (Fig. 8). We also provide a comparison of the discharge amounts provided by each landform proportional to the results of Fig. 12.

The perceptual model illustrates well how steep lateral moraines may provide large water amounts during peak snowmelt or strong rain events in mid-summer, but drain very rapidly in autumn. Talus slopes were not included in the perceptual model, as they play a marginal role in the Otemma catchment and have even faster drainage than steep moraines. On the opposite to steep slopes, the baseflow provided by the bedrock aquifer appears more stable, although its storage decreases by half during winter. In a perspective of future early snowmelt, the model shows that most landforms may become dry much faster, with the exception of i) the outwash plain, which receives water from the glacial stream and ii) the bedrock, which drains slowly; highlighting the future increasing importance of such aquifers to provide wetness and maintain favorable ecological conditions.

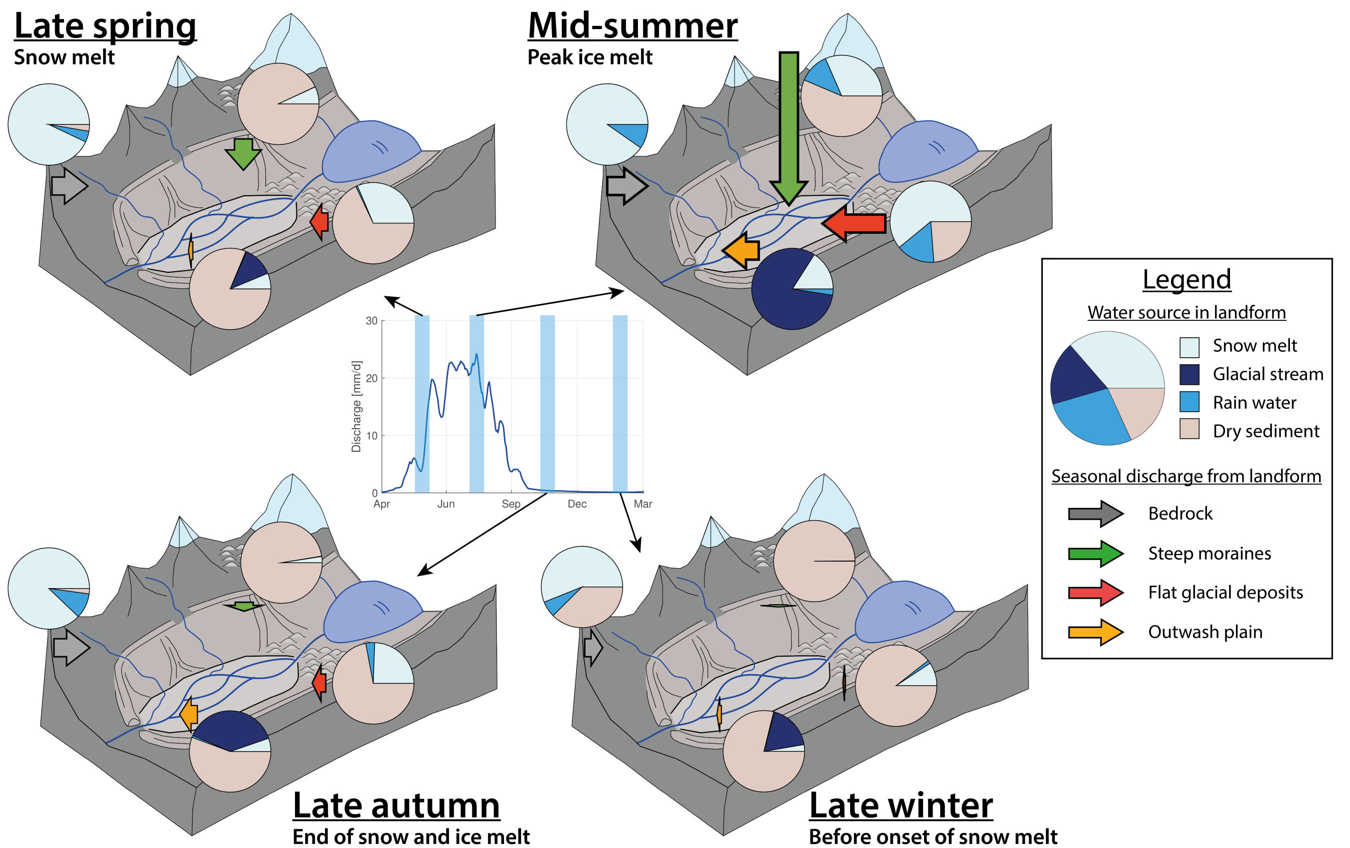


**Figure 13.** Perceptual model of groundwater dynamics in the Otemma catchment during four key hydrological periods. The central hydrograph represents the mean daily catchment-scale river discharge for the year 2015. The pie charts represent the seasonal partitioning of the three water sources (rain water, snowmelt, glacial stream) calculated based on recharge and outflow (Sect. 3.5) for the three main superficial landforms as well as a bedrock aquifer. The source "Glacial stream" represents the mixed discharge leaving the glacier outlet and is an undefined mix of ice- and snowmelt as well as of any liquid rain transiting through the glacier. The share of dry sediments represents the percentage of aquifer storage drained compared to the calculated maximum storage (Sect. 4.4), which is 40 mm for bedrock (missing storage); 23 mm for the steep lateral moraines, 19 mm for flatter glacial deposits and 11 mm for outwash plain. The length of the arrows represents the relative magnitude of the baseflow discharge estimated in Fig. 12 for each landform.

In this representation we also neglected the impact of permafrost melt, although it is likely present at high elevation and in north sloping moraines (Boeckli et al., 2012) and may provide some future additional melt water in glaciated catchment, as shown in the work of (Rogger et al., 2017). Rock glaciers were also not included as their presence is marginal currently in Otemma but their role to store and release water may become increasingly important since they have a capacity to store water on time scales of months as shown in Table 2 and as discussed in more deglaciated catchments in Austria (Wagner et al., 2021).

## 6 Conclusions

This study attempted to bridge the gap between the catchment-scale response of a high elevation glaciated catchment and the hydrological behavior of its landforms, using the case study of a large glacier in the Swiss Alps. The quantitative analyses are simple and are based on a rough estimation of the hydrogeological response of different landforms. Nevertheless, the analysis framework identified the order of magnitude and the timing of the contribution of the different landforms and is readily transposable to other case studies. The resulting perceptual model provides a realistic representation of the main drivers of the groundwater dynamics of the deglaciated zones of glaciated catchments, which can serve as a blueprint for future experimental works as well as for hydrological model development. One clear uncertainty lies in the estimated hydraulic conductivities per landform, in particular their variability in space and depth. In addition, we had to attribute a large part of the groundwater storage to an unidentified compartment, which is likely partially due to a bedrock compartment, but could also be due to a combination of melt water and a subglacial compartment. Future research is needed to specify the very nature of this groundwater storage.

We have shown that superficial geomorphological landforms have a relatively limited capacity to store or release water at time scales longer than a few days, partly because of steep slopes but also due to the generally high hydraulic conductivity. In the future, two main changes can be expected. Firstly, with increasing glacier retreat, the extent of flatter landforms at the valley bottom will increase and may accumulate sufficient sediments to create new outwash plains or flat hummocky moraines that would increase the overall groundwater storage. It remains unclear how much sediments are produced with decreasing glacier volumes and to which extent sediment will be rather deposited or transported more downstream (Lane et al., 2017; Carrivick and Heckmann, 2017). Secondly, with increasing succession time to allow vegetation growth, the formation of soils with enhanced organic matter content and finer soil texture are expected, which will enhance water retention and modify the surface hydraulic conductivity (Hartmann et al., 2020). Recent studies on the evolution of morainic structures have shown that limited changes occurred on time scales smaller than a millennium, with a slight decrease in hydraulic conductivity (Maier et al., 2020, 2021). Thus, the impact of soil-vegetation development on the hydraulic conductivity and the rate of aquifer drainage is likely limited. Nonetheless, early soil development and biofilm growth may start to modify the water retention locally (Roncoroni et al., 2019), promoting more superficial soil moisture, but limiting water infiltration and promoting surface runoffs, which will likely modify groundwater recharge. Finally, the ecological feedback of vegetation development on bank stabilization may also play a role in limiting sediment export and slow geomorphological changes (Miller and Lane, 2018), which may preserve the present geomorphological landforms.

The framework used to analyze the hydrological behavior of selected landforms based on groundwater levels and electric conductivity recordings is readily transferable at relatively low costs to other glaciated catchments. Our EC data underline a large variability between the landforms and spatially across the outwash plain, in addition to strong variations with changing groundwater heads. This observation shows that simple mixing models based on few observations of groundwater electrical conductivity in selected sources are likely not representative of the contribution of each landform and may provide very erroneous estimates of groundwater contribution.

More sophisticated tracer work could complement these analyses in the future. In particular, we think that analysis of stable water isotopes could provide interesting insights into the relative share of subsurface recharge resulting from snow and rain over the season. The use of other geochemical tracers (Hindshaw et al., 2011; Gordon et al., 2015) or even noble gases (Schilling et al., 2021) could provide further insights into the potential contribution from deeper bedrock exfiltration, as well as better constrain the length or travel time of certain groundwater flowpaths.

*Code and data availability.* Field data are available on Zenodo (https://zenodo.org/communities/otemma). Weather data are available under (Müller, 2022a), piezometer data under (Müller, 2022b), river data (Müller and Miesen, 2022) and ERT data under (Müller, 2022c).

The code to reproduce the recession analysis (see Sect. 4.5) was written in matlab using the published data. The codes for the simple storage-discharge model as well as the snow mass balance model (see Sect. 4.4) were written in python using Jupyter Notebook. Both codes are available in supplementary material.

*Author contributions.* T.M. conducted all the data collection and data analysis, produced all the figures and wrote the manuscript draft, including the literature review. B.S. proposed the general research topic and acquired the funding. S.L. and his team organised all field work logistics. B.S. and S.L. jointly supervised the research and edited the manuscript draft version. All authors have read and agreed to the current version of the manuscript.

*Competing interests.* The authors declare that there is no conflict of interest. One co-author is a member of the editorial board of Hydrology and Earth System Sciences.

*Acknowledgements.* The authors also thank Prof. Christophe Lambiel and Prof. James Irving (University of Lausanne) for lending the ERT device as well as Dr. Emily Voytek (University of Lausanne) for acquiring the first ERT data in the Otemma forefield in 2019. T.M. thanks all students and PhD students from the AlpWISE group at University of Lausanne and in particular Floreana Miesen who participated in field data collection at the Otemma glacier forefield. The authors also thank the two anonymous reviewers for their constructive comments to improve this work.

## Appendix A: Diffusion model analysis

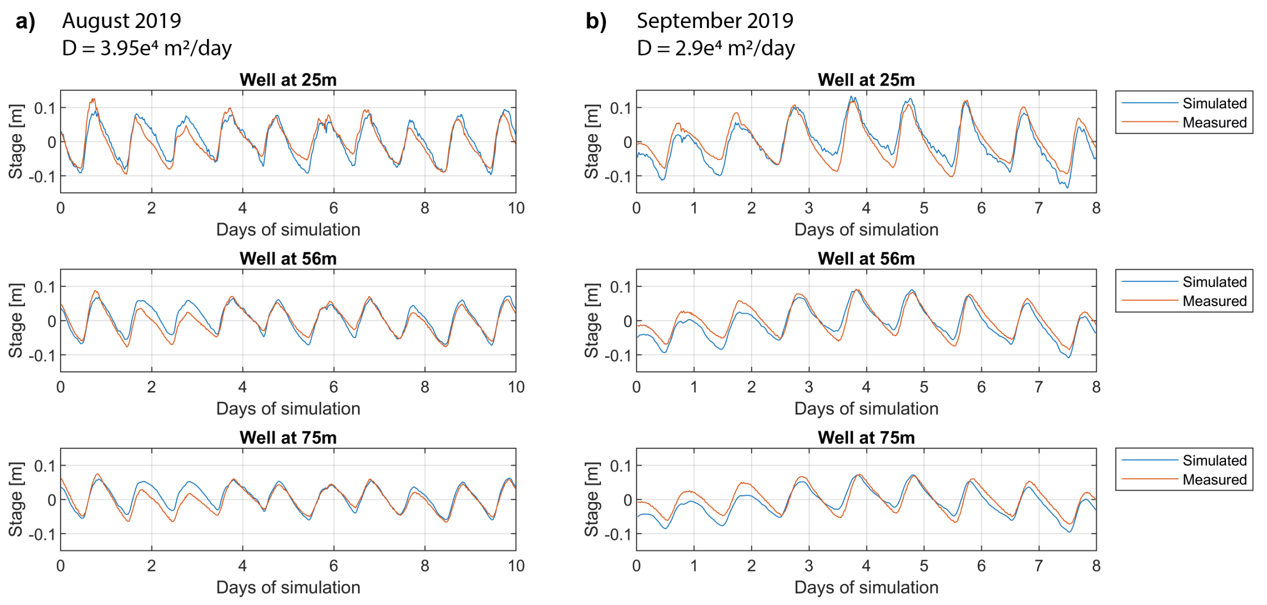


**Figure A1.** Measured and simulated water head variations for piezometers along the downstream transect "$B$" for the best calibration of the diffusion parameter $D$ and for a) the high flow condition in August 2019 and b) lower flow condition in September 2019.

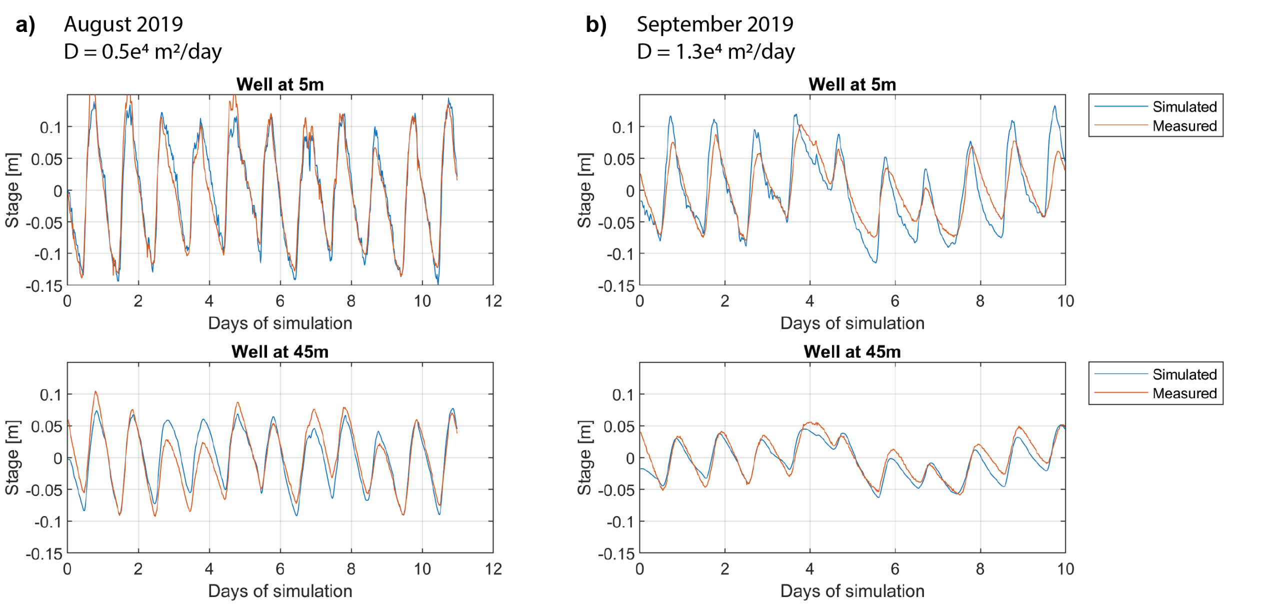


**Figure A2.** Measured and simulated water head variations for piezometers along the upstream transect "$D$" for the best calibration of the diffusion parameter $D$ and for a) the high flow condition in August 2019 and b) lower flow condition in September 2019.

## References


Andermann, C., Longuevergne, L., Bonnet, S., Crave, A., Davy, P., and Gloaguen, R.: Impact of transient groundwater storage on the discharge of Himalayan rivers, Nature Geoscience, 5, 127–132, https://doi.org/10.1038/ngeo1356, 2012.

Ballantyne, C. K.: Paraglacial geomorphology, Quaternary Science Reviews, 21, 1935–2017, https://doi.org/10.1016/S0277-3791(02)00005-7, 2002.

Baraer, M., Mckenzie, J., Mark, B. G., Gordon, R., Bury, J., Condom, T., Gomez, J., Knox, S., and Fortner, S. K.: Contribution of groundwater to the outflow from ungauged glacierized catchments: A multi-site study in the tropical Cordillera Blanca, Peru, Hydrological Processes, 29, 2561–2581, https://doi.org/10.1002/hyp.10386, 2015.

Barandun, M., Huss, M., Usubaliev, R., Azisov, E., Berthier, E., Kääb, A., Bolch, T., and Hoelzle, M.: Multi-decadal mass balance series of three Kyrgyz glaciers inferred from modelling constrained with repeated snow line observations, Cryosphere, 12, 1899–1919, https://doi.org/10.5194/tc-12-1899-2018, 2018.

Benettin, P., Soulsby, C., Birkel, C., Tetzlaff, D., Botter, G., and Rinaldo, A.: Using SAS functions and high-resolution isotope data to unravel travel time distributions in headwater catchments, Water Resources Research, 53, 1864–1878, https://doi.org/10.1002/2016WR020117, 2017.

Beniston, M., Farinotti, D., Stoffel, M., Andreassen, L. M., Coppola, E., Eckert, N., Fantini, A., Giacona, F., Hauck, C., Huss, M., Huwald, H., Lehning, M., López-Moreno, J. I., Magnusson, J., Marty, C., Morán-Tejéda, E., Morin, S., Naaim, M., Provenzale, A., Rabatel, A., Six, D., Stötter, J., Strasser, U., Terzago, S., and Vincent, C.: The European mountain cryosphere: A review of its current state, trends, and future challenges, Cryosphere, 12, 759–794, https://doi.org/10.5194/tc-12-759-2018, 2018.

Berghuijs, W. R., Woods, R. A., and Hrachowitz, M.: A precipitation shift from snow towards rain leads to a decrease in streamflow, Nature Climate Change, 4, 583–586, https://doi.org/10.1038/nclimate2246, 2014.

Berne, A., Uijlenhoet, R., and Troch, P. A.: Similarity analysis of subsurface flow response of hillslopes with complex geometry, Water Resources Research, 41, 1–10, https://doi.org/10.1029/2004WR003629, 2005.

Boeckli, L., Brenning, A., Gruber, S., and Noetzli, J.: Permafrost distribution in the European Alps: Calculation and evaluation of an index map and summary statistics, Cryosphere, 6, 807–820, https://doi.org/10.5194/tc-6-807-2012, 2012.

Boussinesq, J.: Recherches théoriques sur l'écoulement des nappes d'eau infiltrées dans le sol et sur le débit des sources, Journal de Mathématiques Pures et Appliquées, 10, 5–78, http://eudml.org/doc/235283, 1904.

Bovis, M. J.: Rock-slope deformation at Affliction Creek, southern Coast Mountains, British Columbia, Canadian Journal of Earth Sciences, 27, 243–254, https://doi.org/10.1139/e90-024, 1990.

Brighenti, S., Tolotti, M., Bruno, M. C., Wharton, G., Pusch, M. T., and Bertoldi, W.: Ecosystem shifts in Alpine streams under glacier retreat and rock glacier thaw: A review, Science of the Total Environment, 675, 542–559, https://doi.org/10.1016/j.scitotenv.2019.04.221, 2019.

Caballero, Y., Jomelli, V., Chevallier, P., and Ribstein, P.: Hydrological characteristics of slope deposits in high tropical mountains (Cordillera Real, Bolivia), CATENA, 47, 101–116, https://doi.org/10.1016/S0341-8162(01)00179-5, 2002.

Carrivick, J. L. and Heckmann, T.: Short-term geomorphological evolution of proglacial systems, Geomorphology, 287, 3–28, https://doi.org/10.1016/j.geomorph.2017.01.037, 2017.

Carrivick, J. L., Heckmann, T., Turner, A., and Fischer, M.: An assessment of landform composition and functioning with the first proglacial systems dataset of the central European Alps, Geomorphology, 321, 117–128, https://doi.org/10.1016/j.geomorph.2018.08.030, 2018.

Clark, M. P., Rupp, D. E., Woods, R. A., Tromp-van Meerveld, H. J., Peters, N. E., and Freer, J. E.: Consistency between hydrological models and field observations: linking processes at the hillslope scale to hydrological responses at the watershed scale, Hydrological Processes, 23, 311–319, https://doi.org/10.1002/hyp.7154, 2009.

Clow, D., Schrott, L., Webb, R., Campbell, D., Torizzo, A., and Dornblaser, M.: Ground Water Occurrence and Contributions to Streamflow in an Alpine Catchment, Colorado Front Range, Ground Water, 41, 937–950, https://doi.org/10.1111/j.1745-6584.2003.tb02436.x, 2003.

Crossman, J., Bradley, C., Boomer, I., and Milner, A.: Water flow dynamics of groundwater-fed streams and their ecological significance in a glacierized catchment, Arctic, Antarctic, and Alpine Research, 43, 364–379, https://doi.org/10.1657/1938-4246-43.3.364, 2011.

Dewandel, B., Lachassagne, P., Bakalowicz, M., Weng, P., and Al-Malki, A.: Evaluation of aquifer thickness by analysing recession hydrographs. Application to the Oman ophiolite hard-rock aquifer, Journal of Hydrology, 274, 248–269, https://doi.org/10.1016/S0022-1694(02)00418-3, 2003.

Engel, M., Penna, D., Bertoldi, G., Dell'Agnese, A., Soulsby, C., and Comiti, F.: Identifying run-off contributions during melt-induced run-off events in a glacierized alpine catchment, Hydrological Processes, 30, 343–364, https://doi.org/10.1002/hyp.10577, 2016.

Engel, M., Penna, D., Bertoldi, G., Vignoli, G., Tirler, W., and Comiti, F.: Controls on spatial and temporal variability in streamflow and hydrochemistry in a glacierized catchment, Hydrology and Earth System Sciences, 23, 2041–2063, https://doi.org/10.5194/hess-23-2041-2019, 2019.

Fayad, A., Gascoin, S., Faour, G., López-Moreno, J. I., Drapeau, L., Page, M. L., and Escadafal, R.: Snow hydrology in Mediterranean mountain regions: A review, Journal of Hydrology, 551, 374–396, https://doi.org/10.1016/j.jhydrol.2017.05.063, 2017.

Fischer, M., Huss, M., Barboux, C., and Hoelzle, M.: The New Swiss Glacier Inventory SGI2010: Relevance of Using High-Resolution Source Data in Areas Dominated by Very Small Glaciers, Arctic, Antarctic, and Alpine Research, 46, 933–945, https://doi.org/10.1657/1938-4246-46.4.933, 2014.

Flowers, G. E.: Modelling water flow under glaciers and ice sheets, Proceedings of the Royal Society A: Mathematical, Physical and Engineering Sciences, 471, 20140 907, https://doi.org/10.1098/rspa.2014.0907, 2015.

Gabbi, J., Farinotti, D., Bauder, A., and Maurer, H.: Ice volume distribution and implications on runoff projections in a glacierized catchment, Hydrology and Earth System Sciences, 16, 4543–4556, https://doi.org/10.5194/hess-16-4543-2012, 2012.

Gabbi, J., Carenzo, M., Pellicciotti, F., Bauder, A., and Funk, M.: A comparison of empirical and physically based glacier surface melt models for long-term simulations of glacier response, Journal of Glaciology, 60, 1199–1207, https://doi.org/10.3189/2014JoG14J011, 2014.

GLAMOS (1881-2020): The Swiss Glaciers 1880-2018/19, Glaciological Reports No 1-140, Yearbooks of the Cryospheric Commission of the Swiss Academy of Sciences (SCNAT), published since 1964 by VAW / ETH Zurich, https://doi.org/10.18752/glrep_series.

Glas, R., Lautz, L., McKenzie, J., Mark, B., Baraer, M., Chavez, D., and Maharaj, L.: A review of the current state of knowledge of proglacial hydrogeology in the Cordillera Blanca, Peru, WIREs Water, 5, e1299, https://doi.org/10.1002/wat2.1299, 2018.

Gordon, R. P., Lautz, L. K., McKenzie, J. M., Mark, B. G., Chavez, D., and Baraer, M.: Sources and pathways of stream generation in tropical proglacial valleys of the Cordillera Blanca, Peru, Journal of Hydrology, 522, 628–644, https://doi.org/10.1016/j.jhydrol.2015.01.013, 2015.

Grämiger, L. M., Moore, J. R., Gischig, V. S., Ivy-Ochs, S., and Loew, S.: Beyond debuttressing: Mechanics of paraglacial rock slope damage during repeat glacial cycles, Journal of Geophysical Research: Earth Surface, 122, 1004–1036, https://doi.org/10.1002/2016JF003967, 2017.

GTZ: Planning of Water and Hydropower Intake Structures, 1989.

Haeberli, W. and Weingartner, R.: In full transition: Key impacts of vanishing mountain ice on water-security at local to global scales, Water Security, 11, 100 074, https://doi.org/10.1016/j.wasec.2020.100074, 2020.

Hallet, B., Hunter, L., and Bogen, J.: Rates of erosion and sediment evacuation by glaciers: A review of field data and their implications, Global and Planetary Change, 12, 213–235, https://doi.org/10.1016/0921-8181(95)00021-6, 1996.

Harbor, J.: Influence of subglacial drainage conditions on the velocity distribution within a glacier cross section, Geology, 25, 739–742, https://doi.org/10.1130/0091-7613(1997)025<0739:IOSDCO>2.3.CO;2, 1997.

Harman, C. and Sivapalan, M.: A similarity framework to assess controls on shallow subsurface flow dynamics in hillslopes, Water Resources Research, 45, 1–12, https://doi.org/10.1029/2008WR007067, 2009a.

Harman, C. and Sivapalan, M.: Effects of hydraulic conductivity variability on hillslope-scale shallow subsurface flow response and storage-discharge relations, Water Resources Research, 45, 1–15, https://doi.org/10.1029/2008WR007228, 2009b.

Harman, C. J., Sivapalan, M., and Kumar, P.: Power law catchment-scale recessions arising from heterogeneous linear small-scale dynamics, Water Resources Research, 45, 1–13, https://doi.org/10.1029/2008WR007392, 2009.

Harrington, J. S., Mozil, A., Hayashi, M., and Bentley, L. R.: Groundwater flow and storage processes in an inactive rock glacier, Hydrological Processes, 32, 3070–3088, https://doi.org/10.1002/hyp.13248, 2018.

Hartmann, A., Semenova, E., Weiler, M., and Blume, T.: Field observations of soil hydrological flow path evolution over 10 millennia, Hydrology and Earth System Sciences, 24, 3271–3288, https://doi.org/10.5194/hess-24-3271-2020, 2020.

Hauer, F. R., Locke, H., Dreitz, V. J., Hebblewhite, M., Lowe, W. H., Muhlfeld, C. C., Nelson, C. R., Proctor, M. F., and Rood, S. B.: Gravel-bed river floodplains are the ecological nexus of glaciated mountain landscapes, Science Advances, 2, 1–14, https://doi.org/10.1126/sciadv.1600026, 2016.

Hayashi, M.: Alpine Hydrogeology: The Critical Role of Groundwater in Sourcing the Headwaters of the World, Groundwater, 58, 498–510, https://doi.org/10.1111/gwat.12965, 2020.

Heckmann, T. and Morche, D.: Geomorphology of Proglacial Systems, Geography of the Physical Environment, Springer International Publishing, Cham, https://doi.org/10.1007/978-3-319-94184-4, 2019.

Heckmann, T., Mccoll, S., and Morche, D.: Retreating ice: Research in pro-glacial areas matters, Earth Surface Processes and Landforms, 41, 271–276, https://doi.org/10.1002/esp.3858, 2016.

Hindshaw, R. S., Tipper, E. T., Reynolds, B. C., Lemarchand, E., Wiederhold, J. G., Magnusson, J., Bernasconi, S. M., Kretzschmar, R., and Bourdon, B.: Hydrological control of stream water chemistry in a glacial catchment (Damma Glacier, Switzerland), Chemical Geology, 285, 215–230, https://doi.org/10.1016/j.chemgeo.2011.04.012, 2011.

Hogarth, W. L., Li, L., Lockington, D. A., Stagnitti, F., Parlange, M. B., Barry, D. A., Steenhuis, T. S., and Parlange, J.-Y.: Analytical approximation for the recession of a sloping aquifer, Water Resources Research, 50, 8564–8570, https://doi.org/10.1002/2014WR016084, 2014.

Hood, J. L. and Hayashi, M.: Characterization of snowmelt flux and groundwater storage in an alpine headwater basin, Journal of Hydrology, 521, 482–497, https://doi.org/10.1016/j.jhydrol.2014.12.041, 2015.

Hugentobler, M., Loew, S., Aaron, J., Roques, C., and Oestreicher, N.: Borehole monitoring of thermo-hydro-mechanical rock slope processes adjacent to an actively retreating glacier, Geomorphology, 362, 107 190, https://doi.org/10.1016/j.geomorph.2020.107190, 2020.

Huss, M. and Hock, R.: Global-scale hydrological response to future glacier mass loss, Nature Climate Change, 8, 135–140, https://doi.org/10.1038/s41558-017-0049-x, 2018.

Huss, M., Bookhagen, B., Huggel, C., Jacobsen, D., Bradley, R. S., Clague, J. J., Vuille, M., Buytaert, W., Cayan, D. R., Greenwood, G., Mark, B. G., Milner, A. M., Weingartner, R., and Winder, M.: Toward mountains without permanent snow and ice, Earth's Future, 5, 418–435, https://doi.org/10.1002/2016EF000514, 2017.

Immerzeel, W. W., Lutz, A. F., Andrade, M., Bahl, A., Biemans, H., Bolch, T., Hyde, S., Brumby, S., Davies, B. J., Elmore, A. C., Emmer, A., Feng, M., Fernández, A., Haritashya, U., Kargel, J. S., Koppes, M., Kraaijenbrink, P. D. A., Kulkarni, A. V., Mayewski, P. A., Nepal, S., Pacheco, P., Painter, T. H., Pellicciotti, F., Rajaram, H., Rupper, S., Sinisalo, A., Shrestha, A. B., Viviroli, D., Wada, Y., Xiao, C., Yao, T., and Baillie, J. E. M.: Importance and vulnerability of the world's water towers, Nature, 577, 364–369, https://doi.org/10.1038/s41586-019-1822-y, 2020.

Jefferson, A., Nolin, A., Lewis, S., and Tague, C.: Hydrogeologic controls on streamflow sensitivity to climate variation, Hydrological Processes, 22, 4371–4385, https://doi.org/10.1002/hyp.7041, 2008.

Käser, D. and Hunkeler, D.: Contribution of alluvial groundwater to the outflow of mountainous catchments, Water Resources Research, 52, 680–697, https://doi.org/10.1002/2014WR016730, 2016.

Kirchner, J. W.: Catchments as simple dynamical systems: Catchment characterization, rainfall-runoff modeling, and doing hydrology backward, Water Resources Research, 45, https://doi.org/10.1029/2008WR006912, 2009.

Kirchner, J. W., Godsey, S. E., Solomon, M., Osterhuber, R., McConnell, J. R., and Penna, D.: The pulse of a montane ecosystem: Coupling between daily cycles in solar flux, snowmelt, transpiration, groundwater, and streamflow at Sagehen Creek and Independence Creek, Sierra Nevada, USA, Hydrology and Earth System Sciences, 24, 5095–5123, https://doi.org/10.5194/hess-24-5095-2020, 2020.

Klein, G., Vitasse, Y., Rixen, C., Marty, C., and Rebetez, M.: Shorter snow cover duration since 1970 in the Swiss Alps due to earlier snowmelt more than to later snow onset, Climatic Change, 139, 637–649, https://doi.org/10.1007/s10584-016-1806-y, 2016.

Kobierska, F., Jonas, T., Griessinger, N., Hauck, C., Huxol, S., and Bernasconi, S. M.: A multi-method field experiment to determine local groundwater flow in a glacier forefield, Hydrological Processes, 29, 817–827, https://doi.org/10.1002/hyp.10188, 2015a.

Kobierska, F., Jonas, T., Kirchner, J. W., and Bernasconi, S. M.: Linking baseflow separation and groundwater storage dynamics in an alpine basin (Dammagletscher, Switzerland), Hydrology and Earth System Sciences, 19, 3681–3693, https://doi.org/10.5194/hess-19-3681-2015, 2015b.

Kurylyk, B. L. and Hayashi, M.: Inferring hydraulic properties of alpine aquifers from the propagation of diurnal snowmelt signals, Water Resources Research, 53, 4271–4285, https://doi.org/10.1002/2016WR019651, 2017.

Lane, S. N. and Nienow, P. W.: Decadal-Scale Climate Forcing of Alpine Glacial Hydrological Systems, Water Resources Research, 55, 2478–2492, https://doi.org/10.1029/2018WR024206, 2019.

Lane, S. N., Bakker, M., Gabbud, C., Micheletti, N., and Saugy, J. N.: Sediment export, transient landscape response and catchment-scale connectivity following rapid climate warming and Alpine glacier recession, Geomorphology, 277, 210–227, https://doi.org/10.1016/j.geomorph.2016.02.015, 2017.

Langston, G., Bentley, L. R., Hayashi, M., McClymont, A., and Pidlisecky, A.: Internal structure and hydrological functions of an alpine proglacial moraine, Hydrological Processes, 2982, n/a–n/a, https://doi.org/10.1002/hyp.8144, 2011.

Linsbauer, A., Huss, M., Hodel, E., Bauder, A., Fischer, M., Weidmann, Y., Bärtschi, H., and Schmassmann, E.: The New Swiss Glacier Inventory SGI2016: From a Topographical to a Glaciological Dataset, Frontiers in Earth Science, 9, 1–22, https://doi.org/10.3389/feart.2021.704189, 2021.

Mackay, J. D., Barrand, N. E., Hannah, D. M., Krause, S., Jackson, C. R., Everest, J., MacDonald, A. M., and Ó Dochartaigh, B.: Proglacial groundwater storage dynamics under climate change and glacier retreat, Hydrological Processes, 34, 5456–5473, https://doi.org/10.1002/hyp.13961, 2020.

Magnusson, J., Kobierska, F., Huxol, S., Hayashi, M., Jonas, T., and Kirchner, J. W.: Melt water driven stream and groundwater stage fluctuations on a glacier forefield (Dammagletscher, Switzerland), Hydrological Processes, 28, 823–836, https://doi.org/10.1002/hyp.9633, 2014.

Maier, F., van Meerveld, I., Greinwald, K., Gebauer, T., Lustenberger, F., Hartmann, A., and Musso, A.: Effects of soil and vegetation development on surface hydrological properties of moraines in the Swiss Alps, Catena, 187, 104 353, https://doi.org/10.1016/j.catena.2019.104353, 2020.

Maier, F., van Meerveld, I., Meerveld, I., Weiler, M., van Meerveld, I., Meerveld, I., and Weiler, M.: Long-Term Changes in Runoff Generation Mechanisms for Two Proglacial Areas in the Swiss Alps I: Overland Flow, Water Resources Research, 57, 1–30, https://doi.org/10.1029/2021WR030221, 2021.

Maisch, M., Haeberli, W., Hoelzle, M., and Wenzel, J.: Occurrence of rocky and sedimentary glacier beds in the Swiss Alps as estimated from glacier-inventory data, Annals of Glaciology, 28, 231–235, https://doi.org/10.3189/172756499781821779, 1999.

Maizels, J.: Sediments and landforms of modern proglacial terrestrial environments, in: Modern and Past Glacial Environments, 4, pp. 279–316, Elsevier, https://doi.org/10.1016/B978-075064226-2/50012-X, 2002.

Malard, F., Tockner, K., and Ward, J. V.: Shifting dominance of subcatchment water sources and flow paths in a glacial floodplain, Val Roseg, Switzerland, Arctic, Antarctic, and Alpine Research, 31, 135–150, https://doi.org/10.2307/1552602, 1999.

McClymont, A. F., Roy, J. W., Hayashi, M., Bentley, L. R., Maurer, H., and Langston, G.: Investigating groundwater flow paths within proglacial moraine using multiple geophysical methods, Journal of Hydrology, 399, 57–69, https://doi.org/10.1016/j.jhydrol.2010.12.036, 2011.

Miller, H. R. and Lane, S. N.: Biogeomorphic feedbacks and the ecosystem engineering of recently deglaciated terrain, Progress in Physical Geography, 43, 24–45, https://doi.org/10.1177/0309133318816536, 2018.

Milner, A. M., Brown, L. E., and Hannah, D. M.: Hydroecological response of river systems to shrinking glaciers, Hydrological Processes, 23, 62–77, https://doi.org/10.1002/hyp.7197, 2009.

Milner, A. M., Khamis, K., Battin, T. J., Brittain, J. E., Barrand, N. E., Füreder, L., Cauvy-Fraunié, S., Gíslason, G. M., Jacobsen, D., Hannah, D. M., Hodson, A. J., Hood, E., Lencioni, V., Ólafsson, J. S., Robinson, C. T., Tranter, M., and Brown, L. E.: Glacier shrinkage driving global changes in downstream systems, Proceedings of the National Academy of Sciences, 114, 9770–9778, https://doi.org/10.1073/pnas.1619807114, 2017.

Muir, D. L., Hayashi, M., and McClymont, A. F.: Hydrological storage and transmission characteristics of an alpine talus, Hydrological Processes, 25, n/a–n/a, https://doi.org/10.1002/hyp.8060, 2011.

Müller, T.: Weather dataset from Otemma glacier forefield, Switzerland (from 14 July 2019 to 18 November 2021) (v1.2021.02), Zenodo [Data set], https://doi.org/10.5281/zenodo.6106778, 2022a.

Müller, T.: Water table elevation and groundwater temperature from the outwash plain of the Otemma glacier forefield (Switzerland) from 2019 to 2021 (v1.2022.03), Zenodo [Data set], https://doi.org/10.5281/zenodo.6355474, 2022b.

Müller, T.: Electrical Resistivity Tomography (ERT) datasets from the Otemma glacier forefield and outwash plain (v1.2022.03), Zenodo [Data set], https://doi.org/10.5281/zenodo.6342767, 2022c.

Müller, T. and Miesen, F.: Stream discharge, stage, electrical conductivity & temperature dataset from Otemma glacier forefield, Switzerland (from July 2019 to October 2021) (v1.2021.02), Zenodo [Data set], https://doi.org/10.5281/zenodo.6202732, 2022.

Ó Dochartaigh, B. É., MacDonald, A. M., Black, A. R., Everest, J., Wilson, P., Darling, W. G., Jones, L., and Raines, M.: Groundwater–glacier meltwater interaction in proglacial aquifers, Hydrology and Earth System Sciences, 23, 4527–4539, https://doi.org/10.5194/hess-23-4527-2019, 2019.

Oestreicher, N., Loew, S., Roques, C., Aaron, J., Gualandi, A., Longuevergne, L., Limpach, P., and Hugentobler, M.: Controls on Spatial and Temporal Patterns of Slope Deformation in an Alpine Valley, Journal of Geophysical Research: Earth Surface, 126, https://doi.org/10.1029/2021JF006353, 2021.

Parriaux, A. and Nicoud, G.: Hydrological behaviour of glacial deposits in mountainous areas, IAHS Publication 190, 1, 291—-312., http://infoscience.epfl.ch/record/116598, 1990.

Penna, D., Engel, M., Bertoldi, G., and Comiti, F.: Towards a tracer-based conceptualization of meltwater dynamics and streamflow response in a glacierized catchment, Hydrology and Earth System Sciences, 21, 23–41, https://doi.org/10.5194/hess-21-23-2017, 2017.

Planet, T.: Planet Application Program Interface: In Space for Life on Earth, https://api.planet.com, 2017.

Rogger, M., Chirico, G. B., Hausmann, H., Krainer, K., Brückl, E., Stadler, P., and Blöschl, G.: Impact of mountain permafrost on flow path and runoff response in a high alpine catchment, Water Resources Research, 53, 1288–1308, https://doi.org/10.1002/2016WR019341, 2017.

Roncoroni, M., Brandani, J., Battin, T. I., and Lane, S. N.: Ecosystem engineers: Biofilms and the ontogeny of glacier floodplain ecosystems, Wiley Interdisciplinary Reviews: Water, 6, e1390, https://doi.org/10.1002/wat2.1390, 2019.

Rücker, C., Günther, T., and Wagner, F. M.: pyGIMLi: An open-source library for modelling and inversion in geophysics, Computers & Geosciences, 109, 106–123, https://doi.org/10.1016/j.cageo.2017.07.011, 2017.

Rupp, D. E. and Selker, J. S.: Drainage of a horizontal Boussinesq aquifer with a power law hydraulic conductivity profile, Water Resources Research, 41, 1–8, https://doi.org/10.1029/2005WR004241, 2005.

Rupp, D. E. and Selker, J. S.: On the use of the Boussinesq equation for interpreting recession hydrographs from sloping aquifers, Water Resources Research, 42, 1–15, https://doi.org/10.1029/2006WR005080, 2006.

Santos, A. C., Portela, M. M., Rinaldo, A., and Schaefli, B.: Analytical flow duration curves for summer streamflow in Switzerland, Hydrology and Earth System Sciences, 22, 2377–2389, https://doi.org/10.5194/hess-22-2377-2018, 2018.

Schilling, O. S., Parajuli, A., Tremblay Otis, C., Müller, T. U., Antolinez Quijano, W., Tremblay, Y., Brennwald, M. S., Nadeau, D. F., Jutras, S., Kipfer, R., and Therrien, R.: Quantifying Groundwater Recharge Dynamics and Unsaturated Zone Processes in Snow-Dominated Catchments via On-Site Dissolved Gas Analysis, Water Resources Research, 57, 1–24, https://doi.org/10.1029/2020WR028479, 2021.

Somers, L. D., Gordon, R. P., McKenzie, J. M., Lautz, L. K., Wigmore, O., Glose, A. M., Glas, R., Aubry-Wake, C., Mark, B., Baraer, M., and Condom, T.: Quantifying groundwater–surface water interactions in a proglacial valley, Cordillera Blanca, Peru, Hydrological Processes, 30, 2915–2929, https://doi.org/10.1002/hyp.10912, 2016.

Staudinger, M., Stoelzle, M., Seeger, S., Seibert, J., Weiler, M., and Stahl, K.: Catchment water storage variation with elevation, Hydrological Processes, 31, 2000–2015, https://doi.org/10.1002/hyp.11158, 2017.

Stewart, M. K.: Promising new baseflow separation and recession analysis methods applied to streamflow at Glendhu Catchment, New Zealand, Hydrology and Earth System Sciences, 19, 2587–2603, https://doi.org/10.5194/hess-19-2587-2015, 2015.

Temme, A. J. A. M.: The Uncalm Development of Proglacial Soils in the European Alps Since 1850, pp. 315–326, Springer, Cham, https://doi.org/10.1007/978-3-319-94184-4_18, 2019.

Troch, P. A., Berne, A., Bogaart, P., Harman, C., Hilberts, A. G., Lyon, S. W., Paniconi, C., Pauwels, V. R., Rupp, D. E., Selker, J. S., Teuling, A. J., Uijlenhoet, R., and Verhoest, N. E.: The importance of hydraulic groundwater theory in catchment hydrology: The legacy of Wilfried Brutsaert and Jean-Yves Parlange, Water Resources Research, 49, 5099–5116, https://doi.org/10.1002/wrcr.20407, 2013.

Tromp-Van Meerveld, H. J. and McDonnell, J. J.: Threshold relations in subsurface stormflow: 2. The fill and spill hypothesis, Water Resources Research, 42, 1–11, https://doi.org/10.1029/2004WR003800, 2006.

Van Tiel, M., Van Loon, A. F., Seibert, J., and Stahl, K.: Hydrological response to warm and dry weather: do glaciers compensate?, Hydrology and Earth System Sciences, 25, 3245–3265, https://doi.org/10.5194/hess-25-3245-2021, 2021.

Verhoest, N. E. C. and Troch, P. A.: Some analytical solutions of the linearized Boussinesq equation with recharge for a sloping aquifer, Water Resources Research, 36, 793–800, https://doi.org/10.1029/1999WR900317, 2000.

Vincent, A., Violette, S., and Aðalgeirsdóttir, G.: Groundwater in catchments headed by temperate glaciers: A review, Earth-Science Reviews, 188, 59–76, https://doi.org/10.1016/j.earscirev.2018.10.017, 2019.

Vuille, M., Carey, M., Huggel, C., Buytaert, W., Rabatel, A., Jacobsen, D., Soruco, A., Villacis, M., Yarleque, C., Elison Timm, O., Condom, T., Salzmann, N., and Sicart, J. E.: Rapid decline of snow and ice in the tropical Andes – Impacts, uncertainties and challenges ahead, Earth-Science Reviews, 176, 195–213, https://doi.org/10.1016/j.earscirev.2017.09.019, 2018.

Wagener, T., Sivapalan, M., Troch, P., and Woods, R.: Catchment Classification and Hydrologic Similarity, Geography Compass, 1, 901–931, https://doi.org/10.1111/j.1749-8198.2007.00039.x, 2007.

Wagner, T., Kainz, S., Helfricht, K., Fischer, A., Avian, M., Krainer, K., and Winkler, G.: Assessment of liquid and solid water storage in rock glaciers versus glacier ice in the Austrian Alps, Science of The Total Environment, 800, 149 593, https://doi.org/10.1016/j.scitotenv.2021.149593, 2021.

Ward, J. V., Malard, F., Tockner, K., and Uehlinger, U.: Influence of ground water on surface water conditions in a glacial flood plain of the Swiss Alps, Hydrological Processes, 13, 277–293, https://doi.org/10.1002/(SICI)1099-1085(19990228)13:3<277::AID-HYP738>3.0.CO;2-N, 1999.

Winkler, G., Wagner, T., Pauritsch, M., Birk, S., Kellerer-Pirklbauer, A., Benischke, R., Leis, A., Morawetz, R., Schreilechner, M. G., and Hergarten, S.: Identification and assessment of groundwater flow and storage components of the relict Schöneben Rock Glacier, Niedere Tauern Range, Eastern Alps (Austria), Hydrogeology Journal, 24, 937–953, https://doi.org/10.1007/s10040-015-1348-9, 2016.

Wittenberg, H. and Sivapalan, M.: Watershed groundwater balance estimation using streamflow recession analysis and baseflow separation, Journal of Hydrology, 219, 20–33, https://doi.org/10.1016/S0022-1694(99)00040-2, 1999.

Yao, Y., Zheng, C., Andrews, C. B., Scanlon, B. R., Kuang, X., Zeng, Z., Jeong, S. J., Lancia, M., Wu, Y., and Li, G.: Role of Groundwater in Sustaining Northern Himalayan Rivers, Geophysical Research Letters, 48, 1–10, https://doi.org/10.1029/2020GL092354, 2021.

Zuecco, G., Carturan, L., De Blasi, F., Seppi, R., Zanoner, T., Penna, D., Borga, M., Carton, A., and Dalla Fontana, G.: Understanding hydrological processes in glacierized catchments: Evidence and implications of highly variable isotopic and electrical conductivity data, Hydrological Processes, 33, 816–832, https://doi.org/10.1002/hyp.13366, 2019.